HYDROTHERMAL CONVERSION OF DIATOM FRUSTULES INTO BARIUM TITANATE BASED REPLICAS

A Thesis
Presented to
The Academic Faculty

By

Eric Ernst

In Partial Fullfillment
Of the Requirements for the Degree
Master of Science in the
School Materials Science and Engineering

Georgia Institute of Technology

July 2007

HYDROTHERMAL CONVERSION OF DIATOM FRUSTULES INTO BARIUM TITANATE BASED REPLICAS

Approved By:

Dr. Kenneth H. Sandhage, Advisor
School of Materials Science and Engineering
Georgia Institute of Technology

Dr. Robert L. Snyder, Chair, Advisor
School of Materials Science and Engineering
Georgia Institute of Technology

Dr. Thomas H. Sanders, Jr.
School of Materials Science and Engineering
Georgia Institute of Technology

Date Approved: June 22, 2007

Acknowledgements

This work would not have been possible without the encouragement and support of many people in my life including my family, friends, and faculty at Georgia Tech. I greatly appreciate the financial, research, and academic support from both of my advisors, Dr. Ken H. Sandhage and Dr. Robert L. Snyder. I also thank Dr. Snyder for taking me on as one of his graduate students and helping me to join Dr. Sandhage's research group. In parallel, I thank Dr. Sandhage for allowing me to join his dedicated team of graduate students and post-docs. Without the help of group members Matt Dickerson, Sam Shian, Mike Weatherspoon, Zhihao Bao, Phillip Graham, Dave Lipke, and Christopher Gaddis, I would not have been able to complete this work.

I would also like to thank Michael Haluska for X-ray diffraction training and analysis assistance. Yunshu Zhang for his assistance in the laboratory. Ye Cai for his assistance with microscopy analysis.

Special thanks to my fiancé, Sarah Vantine for her endless encouragement during my years in graduate school. And to my parents for their support and never giving up hope while trying to led me down a path to success.

TABLE OF CONTENTS

LIST OF TABLES

LIST OF FIGURES

Summary

Numerous organisms produce ornately detailed inorganic structures (often known as shells) with features on length scales from the nanoscale to the microscale. One organism, commonly referred to as a diatom, originates from algae and is found throughout the oceans on Earth. These diatoms possess skeletal structures, frustules, made from silicon dioxide. This chemical makeup limits the number of possible applications for which these structures can be used.

Using a series of gas displacement reactions, these frustules can be converted to other useful materials, such as magnesium oxide and titanium dioxide, while maintaining the features of the frustule template. In the current research, silicon dioxide frustules were converted to titanium dioxide replicas using method previously devised by our group. The titanium dioxide replicas were subjected to a hydrothermal reaction by exposing the replicas to an aqueous basic solution containing barium hydroxide to form barium titanate and barium strontium titanate replicas. The effects of reaction temperature, time, and solution composition on extent of conversion were examined. The conventional method of converting titanium dioxide to barium titanate, using a convection heating oven, was compared with a microwave assisted heating method to study the advantages of using microwave heating over convection heating.

Chapter 1

Enhanced Hydrothermal Conversion of Surfactant-modified Diatom Microshells into Barium Titanate Replicas

1.1 Introduction

The attractive electronic, optical, and chemical properties exhibited by barium titanate-based compositions have led to the use of these ceramics as capacitors, thermistors, actuators, sensors, phosphors, and other devices.[1-8] A variety of approaches (e.g., mixed oxide, mixed salt, sol-gel, polymeric precursor, hydrothermal, microemulsion, mechanochemical, combustion syntheses) have been used to synthesize $BaTiO_3$ powders with fine particle and crystal sizes.[9-19] Nanocrystalline barium titanate-based ceramics have exhibited relatively high room temperature dielectric constants that are temperature- and voltage-stable for integrated capacitors[20,21], high sensitivity to water vapor and carbon dioxide for gas sensors[22-24], and enhanced response of fluorescence to temperature changes for real-time temperature monitoring.[25] The worldwide interest in nanoscale ferroelectric devices has also led to the recent syntheses of $BaTiO_3$ nanowires[26], nanorods[27], nanoshell tubes[28], and nanoshell spheres.[29,30] However, the scalable fabrication of complex three-dimensional (3-D) $BaTiO_3$-based nanostructures in a variety of well-controlled morphologies via synthetic methods has been a significant challenge.

Nature, on the other hand, provides impressive examples of 3-D microscale to nanoscale mineral assembly.[31-39] For example, coccolithophorids (*Haptophyta*) and diatoms (*Bacillariophyta*) are single-celled algae that assemble intricate nanostructured

calcium carbonate and silica microshells, respectively.[35-40] A particularly wide variety of morphologies can be found among the microshells (frustules) of the estimated 10^5 species of diatoms.[40,41] Each species of diatom assembles an amorphous silica-based frustule with a particular 3-D shape and a specific pattern of nanoscale features (e.g., nanoscale pores, channels, ridges, tubules).[38-40] The sustained reproduction of a given diatom species can yield enormous numbers of diatom cells with the same 3-D frustule shape.[42,43] Such intricate, genetically-precise, and massively-parallel 3-D self-assembly under ambient conditions has no analog in man-made processing. Continued progress in the genetic modification of diatoms promises to yield frustules with shapes tailored for specific applications (i.e., genetically-engineered micro/nanodevices).[44-47] However, the natural silica-based chemistry of diatom frustules limits the range of such potential applications.

Silica-based diatom frustules can be converted into replicas comprised of other non-silica-bearing oxides through the use of gas/silica displacement reactions (i.e., via the patented Bioclastic and Shape-preserving Inorganic Conversion or BaSIC process).[48-53] For example, the following net metathetic reaction was first proposed for replacing the silica in diatom frustules with titania.[49]

$$TiF_4(g) + SiO_2(s) => TiO_2(s) + SiF_4(g) \quad (1.1)$$

Subsequent work by Unocic, et al.[51] demonstrated that an intermediate reaction product, $TiOF_2(s)$, forms in advance of titania by the following reaction.

$$2TiF_4(g) + SiO_2(s) => 2TiOF_2(s) + SiF_4(g) \quad (1.2)$$

With proper control of the TiF_4:SiO_2 reactant ratio and temperature, these authors generated $TiOF_2$-based structures that retained the 3-D shapes and fine features of the

starting silica frustules.[51] The conversion of $TiOF_2$ into TiO_2 can then be conducted by reactions of the following type.[51,54-56]

$$TiOF_2(s) + 1/2O_2(g) \Rightarrow TiO_2(s) + F_2(g) \quad (1.3a)$$

$$TiOF_2(s) + H_2O(g) \Rightarrow TiO_2(s) + 2HF(g) \quad (1.3b)$$

Unfortunately, the standard Gibbs free energy of formation of solid $TiOF_2$, $\Delta G^o_f[TiOF_2(s)]$, at $\leq 350^oC$ is not available in common thermodynamic tables (nor apparently in the literature) to allow for thermodynamic calculation of the critical $(O_2)^{1/2}$:F_2 and H_2O:$(HF)^2$ ratios required to enable reactions (3a) and (3b) to proceed spontaneously to the right (note: although Dudley, et al.[66] recently suggested that reaction (3a) was thermodynamically unfavored, the value of $\Delta G^o_f[TiOF_2(s)]$, or a source of such data, was not provided to allow for calculation of the critical $(O_2)^{1/2}$:F_2 ratio). Nonetheless, both reactions have been successfully conducted at modest temperatures (i.e., $\leq 350^oC$) with flowing oxygen or moist air.[51,54-56]

Coating-based approaches may also be used to alter the chemistries of diatom frustules.[57-65] If the coating is thin, continuous, conformal, rigid, and chemically robust, then silica-free structures (e.g., zirconia or polymer[59,63]) possessing the external shape of the starting frustule can be produced upon selective dissolution of the underlying silica frustule (note: if the internal and external surfaces of the frustule are coated, then dissolution of the silica will yield a hollow wall structure). Weatherspoon, et al. synthesized the first freestanding barium titanate-based frustule structures by using a sol-gel process to generate a conformal and continuous $BaTiO_3$ coating at 700^oC on chemically-compatible magnesia-converted frustule replicas (formed through reaction

with magnesium gas[48-50,52]).[56,61,64] Selective dissolution of the underlying magnesia then yielded freestanding phase-pure $BaTiO_3$ structures that retained the 3-D frustule shape.[56]

Combination of gas/solid and liquid/solid reactions is examined for the low-temperature syntheses of $BaTiO_3$ replicas of diatom frustules. With this approach, silica-based frustules are first converted into titania replicas via reactions (2)-(3b) above (as per Unocic, et al.[51]) and then converted into barium titanate replicas via hydrothermal reaction with barium hydroxide-bearing aqueous solutions, as indicated below.

$$TiO_2(s) + \{Ba(OH)_2\} \Rightarrow BaTiO_3(s) + H_2O(l) \quad (1.4)$$

where $\{Ba(OH)_2\}$ refers to barium hydroxide dissolved within water. Such reactions allow for the syntheses of barium titanate replicas at lower reaction temperatures than for sol-gel-based approaches, and could yield solid wall replicas of the frustules (as opposed to hollow wall structures that are produced with coating-based methods, upon removal of the silica). The partial hydrothermal conversion of titania frustule replicas into barium titanate was initially examined by Gaddis[65], and has since been reported by Cai, et al.[56] Dudley, et al.[66] have recently also reported the partial conversion of TiO_2 frustule replicas (synthesized by the method of Unocic, et al.[51,56]) into $BaTiO_3$ via reaction of liquid $Ba(OH)_2 \cdot 8H_2O$ at 120°C for 10 h. The purpose of this chapter is to evaluate the use of a surfactant-based dissolution/reprecipitation process to significantly enhance the exposed surface areas of silica diatom frustules, and thereby reduce the time required for complete hydrothermal conversion into barium titanate replicas.

1.2 Experimental Materials and Procedure

The starting diatom frustules (obtained as flame-polished diatomaceous earth, DE, from a commercial vendor) used in the present work, possessed hollow cylindrical shapes and were decorated with rows of fine (several hundred nm diameter) pores (Figure 1.1). Nitrogen adsorption analysis (BET, Autosorb-1, Quantachrome, Boynton Beach, FL) of DE yielded a modest surface area of 1.6 m^2/g. The first step for the comparison was a surface treatment of the DE.

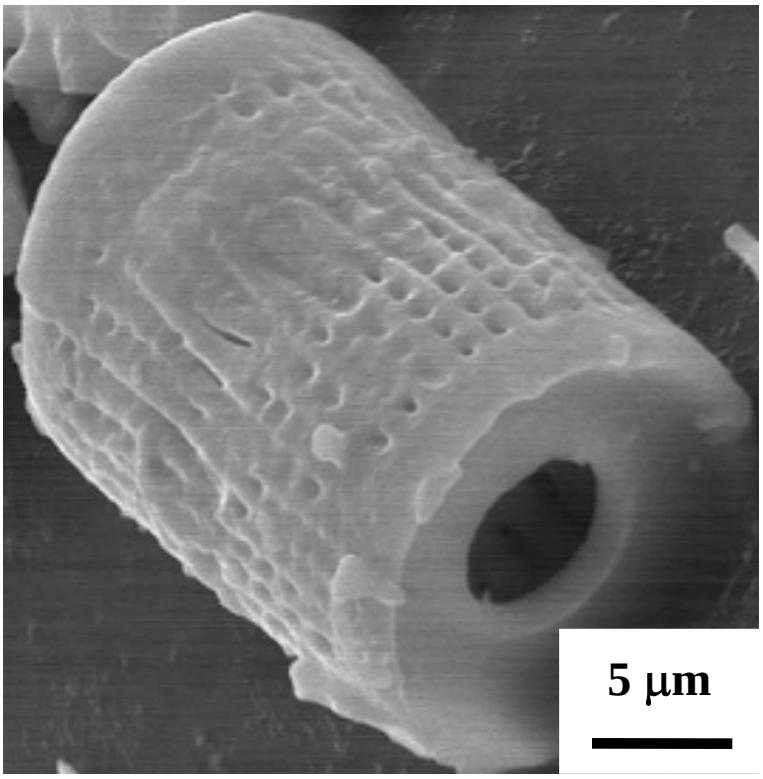

Figure 1.1 Secondary electron image of an unmodified, *Aulacosira* diatomaceous earth microshell.

1.2.1 CTAB Treatment of Diatomaceous Earth

The specific surface area of the diatomaceous earth was significantly enhanced when exposed to a surfactant-induced dissolution/reprecipitation treatment similar to that reported by Fowler, et al.[67] Because the treatment is at elevated temperatures and pressures, a suitable reaction vessel is needed to ensure minimal loss of water or solution. Due to the properties of the CTAB, the reaction was performed in a more confined space when compared to that of Fowler, et al.[67]

A basic aqueous solution of sodium hydroxide (NaOH) was created by dissolving 0.845 g of NaOH pellets into 30 ml of deionized water to achieve a 0.7 molarity. The pellets were stirred for 5 min until they were completely dissolved. 3.05 g of (1-exadecyl)trimethylammonium bromide (CTAB, $CH_3(CH_2)_{15}N(Br)(CH_3)_3$, Alfa Aesar, Ward Hill, MA) was added to the basic solution using a spatula. To ensure complete dissolution, the solution was stirred for another 15 min. A 5.0 g batch of DE was then added to this solution (i.e., a 10:1 SiO_2:CTAB molar ratio). After stirring for 15 min, the slurry was transferred to a 50 mL (2.4 cm I.D. × 15.2 cm L) stainless steel container and sealed hand tight. The container was then placed in an oven preheated to 112^{o}C. After 72 h, the container was removed and allowed to cool under atmospheric conditions. Upon cooling, the sample was washed (Nalgene filter) using a 46 mm diameter, 0.8 μm filter cellulose membrane and protective adsorbent pad (Pall). During washing, the water formed bubbles after passing through the filter indicating the presence of CTAB. Therefore, the frustules were washed until the bubbles were no longer present. After filtering, and thorough washing with deionized water, the frustules were heated in air at

1^{o}C/min to 540^{o}C and held for 10 min (for drying and pyrolysis of residual organic material).

A secondary electron image of a CTAB-treated microshell is shown in Figure 1.2. The microscale 3-D frustule morphology and surface features did not appear to be altered by this treatment. However, BET analysis indicated that the DE surface area increased by a factor of 75 to a value of 120 m^2/g.

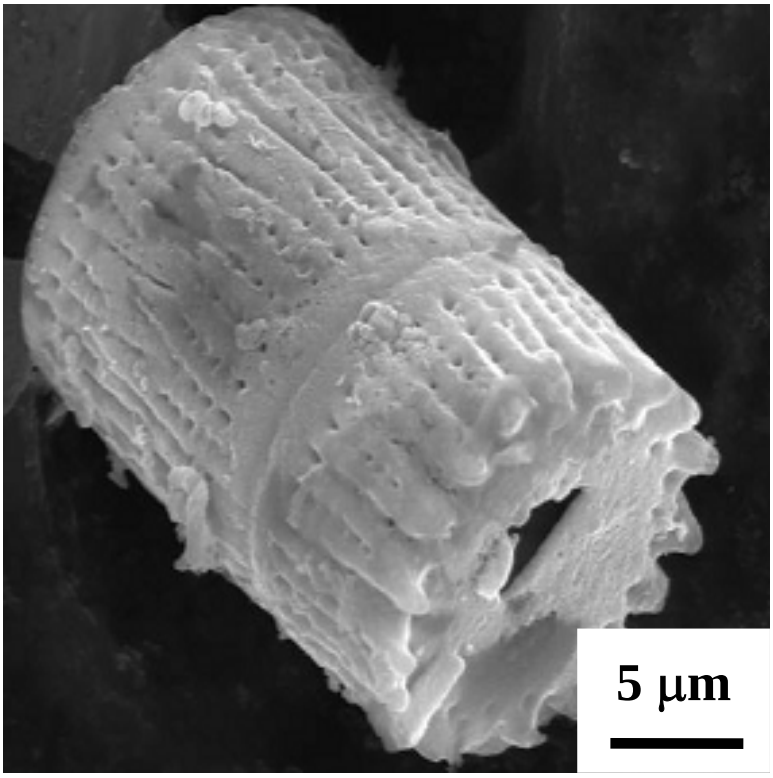

Figure 1.2 Secondary electron image of a CTAB-treated *Aulacosira* diatomaceous earth microshell

1.2.2 Conversion of frustules from SiO_2 to TiO_2

The CTAB-treated and untreated diatom frustules were converted into anatase phase TiO_2 using the method of Unocic et al.[51] In a glove box with an argon controlled environment, 1.0 g of TiF_4 (titanium(IV) fluoride, Advanced Chemicals Research, Tulsa

OK) was placed in one end of a titanium tube (2.35 cm I.D., 17 cm long, Grade 2, Titanium Industries, Rockway, NJ USA) in which a 1.25 cm segment (from the end of the tube) was precrimped and welded shut by method of tungsten inert gas welding (TIG). Next, 0.2 g of SiO_2 frustules were evenly distributed into a homemade nickel tray (6.5 cm long x 1.8 cm wide x 0.6 cm deep) with a powder bed height of less than 1 mm. The nickel tray was placed inside the tube and centered on the length. A press was used to crimp the open end of the vessel 1.25 cm from the end. The crimped opening was TIG welded shut and the tube removed from the glove box.

The sealed tube was transferred to a furnace and heated at 5 ºC/min to 350 ºC for a duration of 2 h. After heat treatment, the tube was opened and the newly formed sample of $TiOF_2$ frustules was transferred to a MgO bowl (magnesium oxide, 2.54 cm diameter, 1.25 cm deep, Ozark Technical Ceramics). The $TiOF_2$ frustules were transferred back to the furnace for further heat treatment using a ramp rate of 5 ºC/min and holding at 400 ºC for 5 h. A humid atmosphere was produced by flowing O_2 (oxygen gas) at 1 mL/min through a flask of 70ºC deionized water prior to introduction to the furnace. In order to maintain an atmospheric O_2 partial pressure, a flask was used at the outlet of the furnace.

X-ray diffraction analysis indicated that this treatment resulted in complete conversion of the silica frutules into the anatase polymorph of titania (Figure 1.3). A secondary electron image of a titania/microshell from CTAB-treated DE is shown in Figure 1.4 (a similar microscale morphology was observed for the non-CTAB-treated, titania-converted specimens). The cylindrical 3-D morphology of the starting microshell was preserved in the titania replicas.

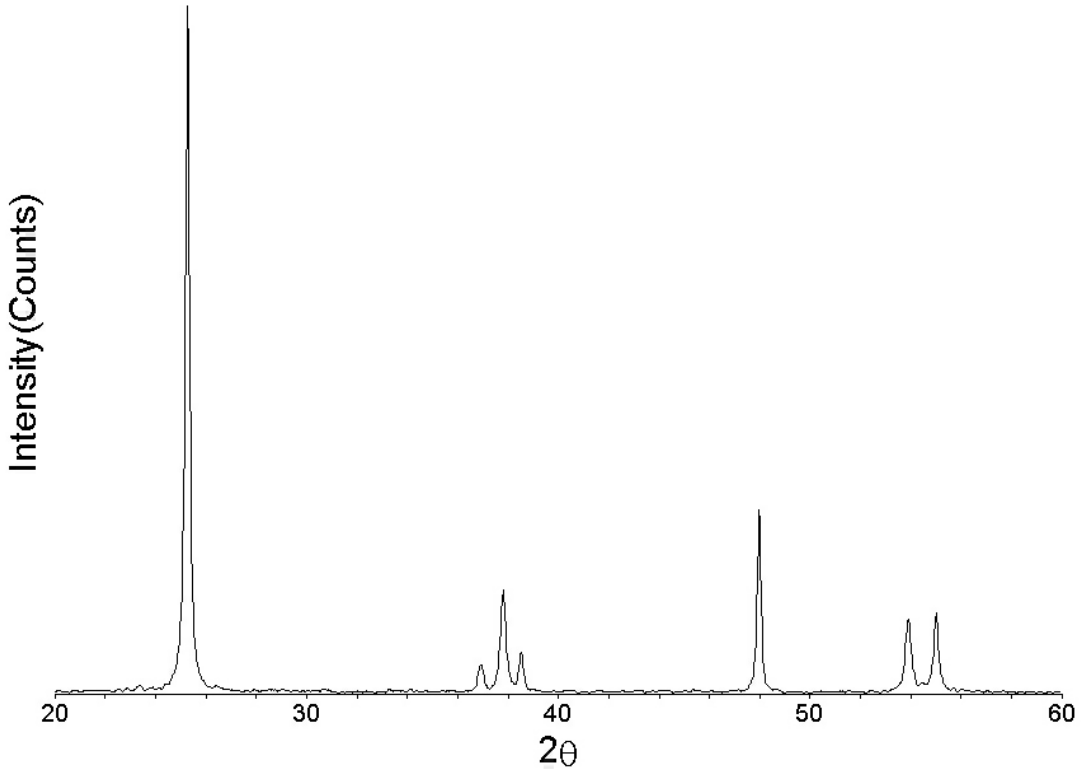

Figure 1.3 XRD pattern of anatase phase TiO_2 diatom replicas

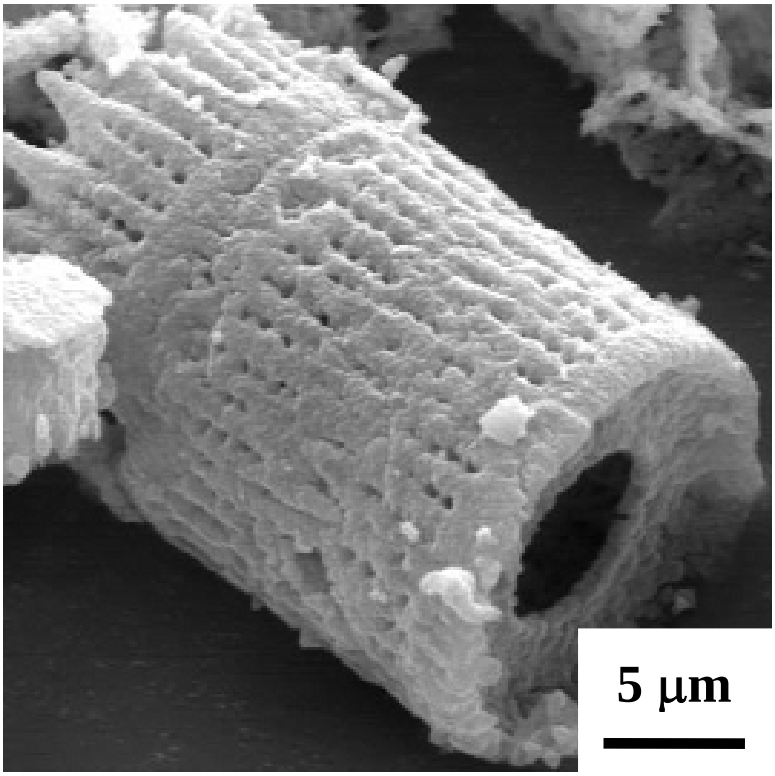

Figure 1.4 Secondary electron image of a CTAB-treated microshell after conversion to TiO_2.

BET analyses indicated that the titania frustule replicas generated from non-CTAB-treated and CTAB-treated silica frustules possessed specific surface areas of 5.2 and 11.3 m^2/g, respectively. The specific surface area of the titania replicas synthesized from CTAB-treated silica was significantly lower than for the CTAB-treated silica (11.3 vs. 120 m^2/g). This decrease is likely to have resulted from the loss of fine (< 4 nm) pores present in the CTAB-treated silica upon conversion into titania. Barrett-Joyner-Halenda analysis[68] (BJH) of the nitrogen desorption curves indicated that the CTAB-

treated silica possessed a significant amount of mesoporosity; that is, pores $\leq$ 4 nm in diameter comprised 68% of the cumulative volume occupied by all pores $\leq$ 50 nm in diameter (Figure 1.5, a and b). However, BJH analysis of the titania replicas generated from the CTAB-treated silica indicated that pores $\leq$ 4 nm in diameter comprised only 8.7% of the cumulative volume occupied by all pores $\leq$ 50 nm in diameter (Figure 1.6, a and b).

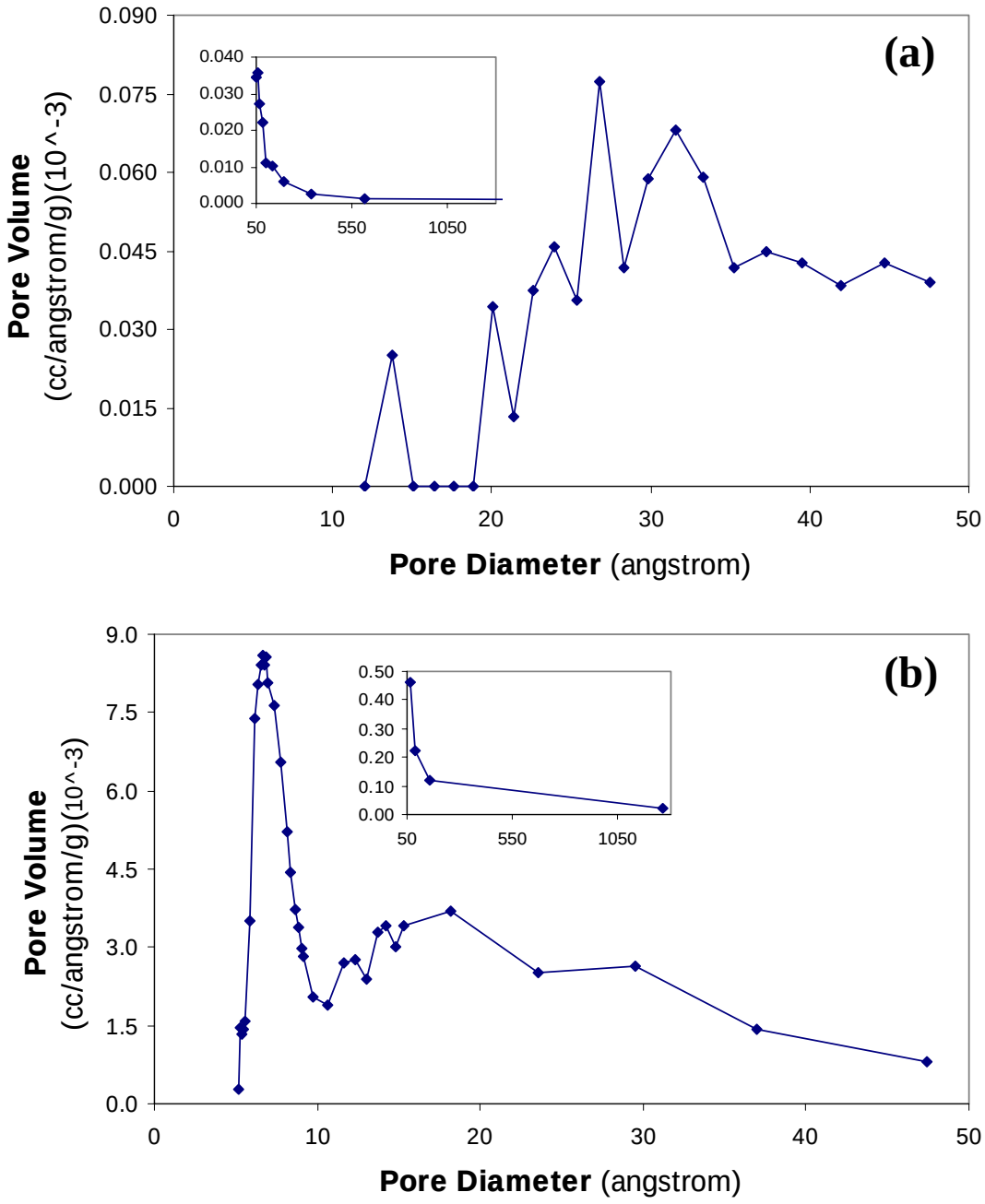

Figure 1.5 BJH pore size distributions for: (a) non-CTAB treated frustules, and (b) CTAB treated frustules.

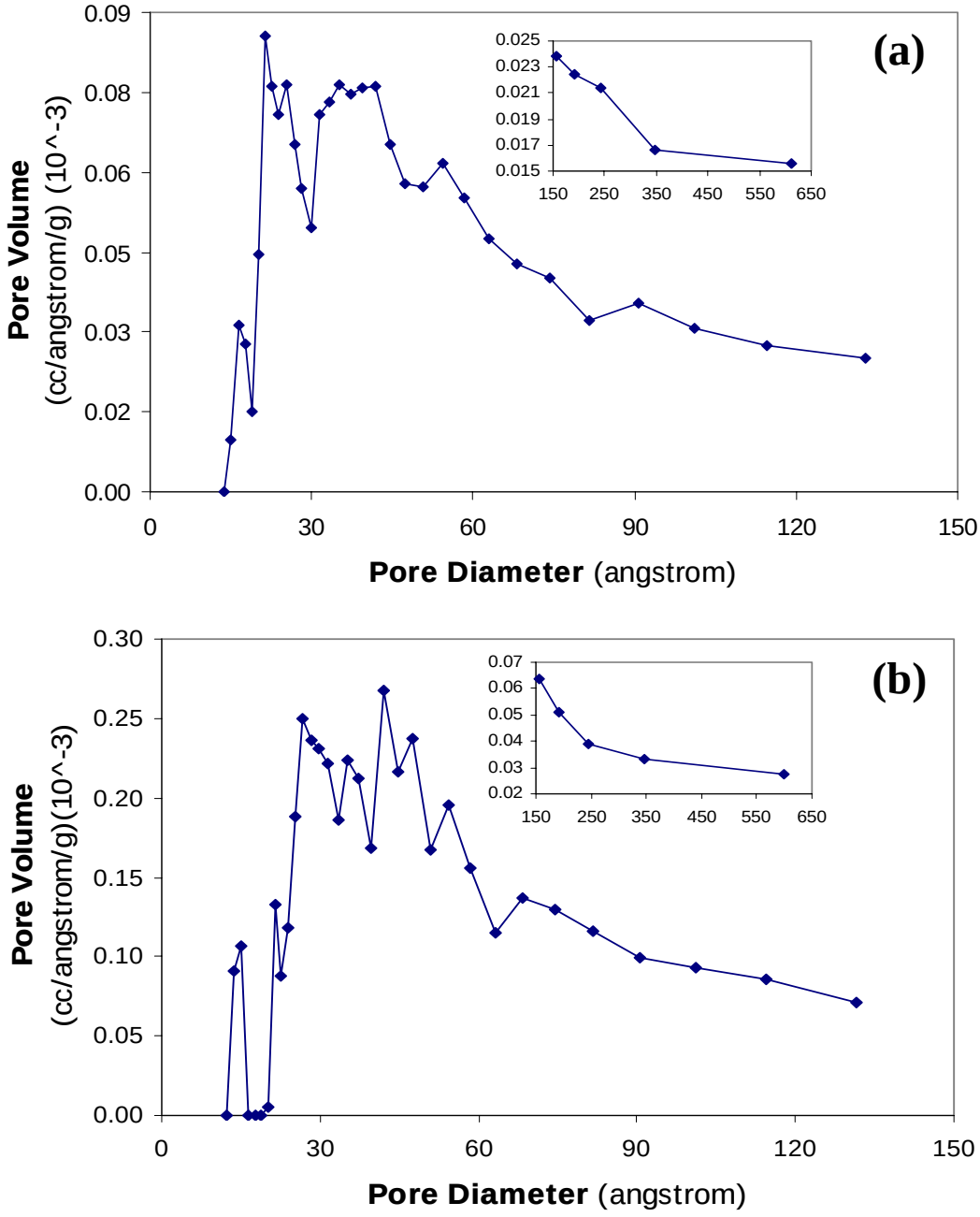

Figure 1.6 BJH pore size distributions for: (a) non-CTAB treated frustules after conversion to TiO_2, and (b) CTAB treated frustules after conversion to TiO_2.

1.2.3 Hydrothermal Conversion of frustules from TiO_2 to $BaTiO_2$

For hydrothermal conversion into barium titanate, 0.050 g of titania frustule replicas, 0.60 g of barium hydroxide octahydrate ($Ba(OH)_2 \cdot 8(H_2O)$, >98% purity, Alfa Aesar), and 0.60 mL of de-ionized water (i.e., a molar $Ba(OH)_2 \cdot 8(H_2O):TiO_2:H_2O$ ratio of 3.0:1:53) were placed in a tube machined from a PTFE rod (12.5 mm internal dia., 21 mm internal length, Virgin Electrical Grade PTFE, McMaster-Carr). Such charged tubes were sealed with PTFE plugs within an argon atmosphere glove box. The sealed tubes were thrust into an oven preheated to 100°C, and held at this temperature for times up to 48 h. There was no change in weight observed for any of the tubes. Upon cooling and filtration, the reacted frustules were washed 8 times with de-ionized water heated to 75°C to remove residual barium hydroxide adhering to the specimen. The reacted frustules were then placed in an ultrasonic cleaner (Model 2510, Branson, Danbury, CT) for 1 h to dislodge any remaining barium hydroxide adhering to the specimens. After ultrasonication, the reacted frustules were again washed 8 times with heated de-ionized water. The frustules were then dried at 75°C for 24 h.

1.2.4 $BaTiO_3/TiO_2$ Mixed Oxide Standards

Mixed oxides of cubic phase $BaTiO_3$ powder (Sigma Aldrich) and anatase phase TiO_2 (Alpha Aesar) were made to quantify of the amount of conversion from TiO_2 to $BaTiO_3$. Table 1.1 lists the compositions of the 12, 1 g mixtures of $BaTiO_3$ and TiO_2 that were made ranging from 10 to 99 weight percent $BaTiO_3$. Each powder was weighed together in the mortar where they would be mixed to ensure no loss of powder in transferring from a weigh vessel. The powders were mixed for 15 min in a slurry with

acetone. The mortar was then placed on a hot plate to evaporate the acetone. After drying, the sample was transferred to a glass vial and placed in a dry oven at 85 ºC for 24 h to ensure complete evaporation of acetone.

Table 1.1 Weights of $BaTiO_3$ and TiO_2 powders used for quantitative wt. % analysis of $BaTiO_3$ in the specimens.

Weight % $BaTiO_3$	*$BaTiO_3$ (mg)*	*TiO_2 (mg)*
10	100	900
20	200	800
30	300	700
40	400	600
50	500	500
60	600	400
70	700	300
80	800	200
90	900	100
95	950	50
97	970	30
99	990	10

After the drying, XRD analysis was performed on each mixture (Figure 1.7). Using an XRD analysis program (*Jade 7 XRD Pattern Processing Identification & Quantification)*, the ratio of the (110) peak for $BaTiO_3$ to the (101) peak for anatase TiO_2

was calculated for each mixture. The ratio of the peak areas were normalized to the ratio for the mixture containing 99.0 weight % $BaTiO_3$ and plotted against the known weight percents of $BaTiO_3$ for the mixtures (Figure 1.8).

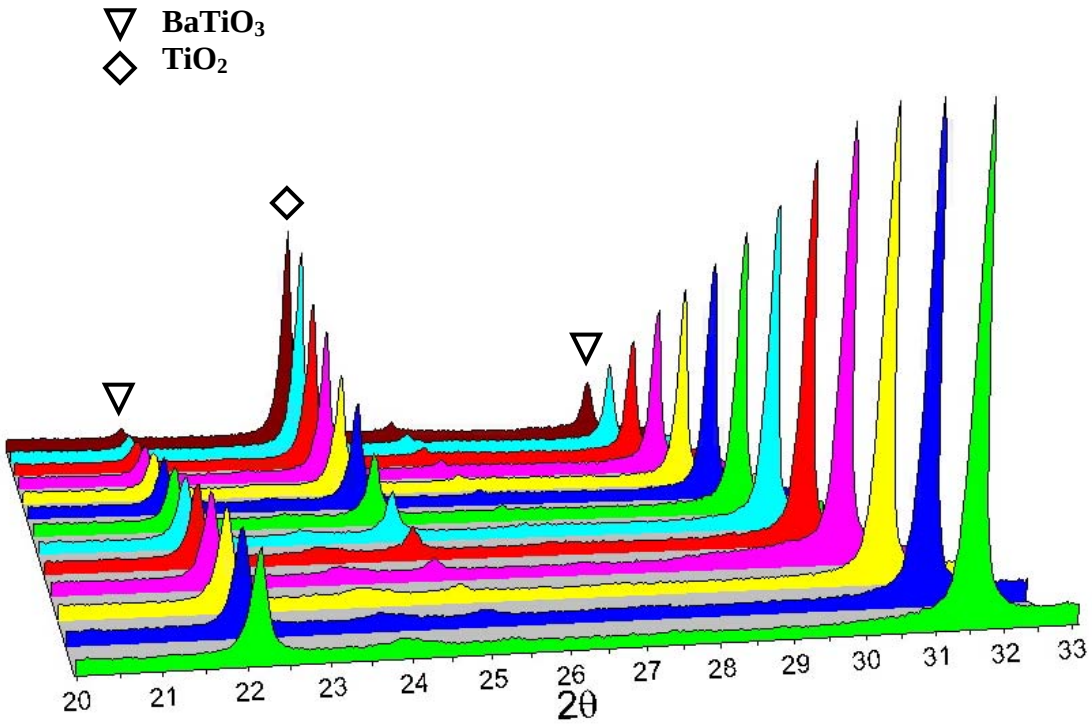

Figure 1.7 3-D overlay of the XRD patterns for the $BaTiO_3/TiO_2$ mixed oxide compositions with weight ratios ranging from 10 mg $BaTiO_3$ and 900mg of TiO_2 to 990mg $BaTiO_3$ and 10 mg TiO_2 (background to foreground respectively).

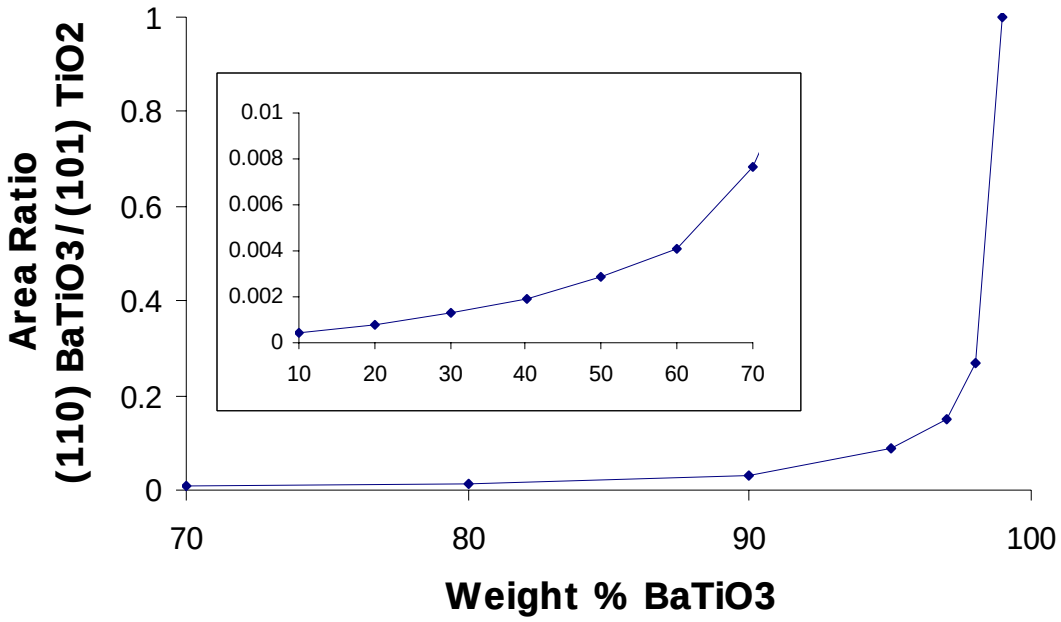

Figure 1.8 Plot illustrating the correlation between XRD peak area ratios for the main peaks of $BaTiO_3$ and TiO_2 to the known weight percents of $BaTiO_3$. The ratios have been normalized to the 99.0 weight percent $BaTiO_3$ ratio.

The crystallite size and morphology of the reacted frustules was investigated by SEM (S-800, Hitachi, Japan). The composition of the frustules was studied with X-ray diffraction (Alpha-1, Panalytical, Netherlands) and energy dispersive spectroscopy (EDS). Crystallite size was calculated from XRD using Scherrer analysis to extract crystallite size information from XRD peak widths, which does not require the use of a coarse-grained standard material.[69] Scherrer analysis measures the XRD peak width (B) for all peaks for a phase. The term, B*cos (θ), is plotted versus the term, sin (θ). A linear regression is used to fit the points. The particle size and strain were then calculated from the y-intercept and slope of the linear fit, respectively. The particle size is given as D.

$$B*\cos(\theta) = 0.9\lambda / D$$

1.3 Results and Discussion

XRD analyses obtained after hydrothermal reaction of the non-CTAB-treated and CTAB-treated titania replicas for various times at 100°C are shown in Figures 1.9, a-c and d-f, respectively. After 8 h of reaction, both types of specimens consisted of appreciable amounts of $BaTiO_3$ and TiO_2 (anatase). A substantial reduction in the amount of residual TiO_2 occurred between 8 and 24 h of reaction. The ratios of the areas of the most intense (110) $BaTiO_3$ and (101) TiO_2 diffraction peaks for the two types of specimens and for different reaction times are shown in Table 1.2. After 8 h and 24 h of reaction, the $BaTiO_3$:TiO_2 peak area ratio was higher for the CTAB-treated specimens than for the non-CTAB-treated specimens. After 48 h of reaction, a detectable diffraction peak for TiO_2 (i.e., the (101) diffraction peak located near 25.3 degrees) was observed in the non-CTAB-treated specimen, whereas this peak was almost absent in the CTAB-treated specimen.

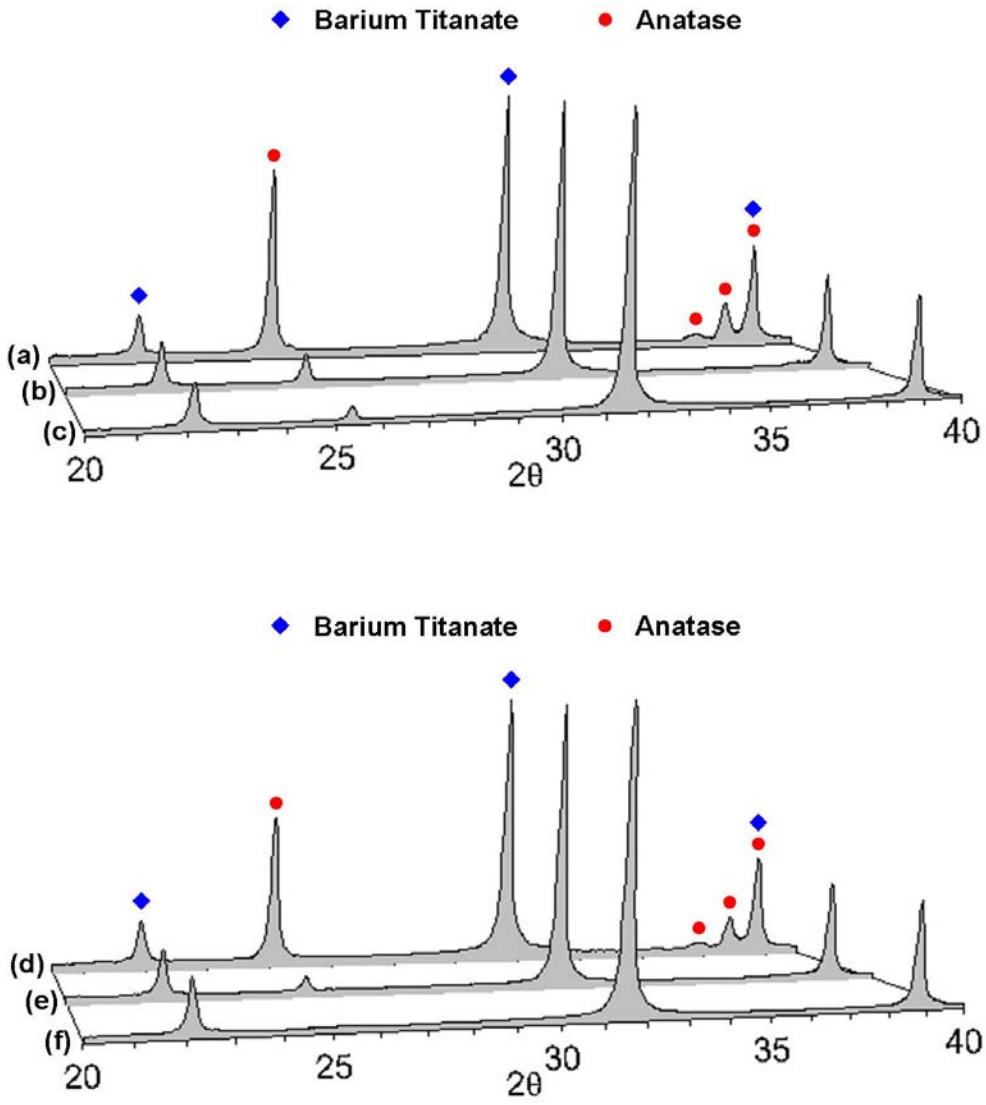

Figure 1.9 X-ray diffraction patterns obtained from frustule specimens after various hydrothermal reaction times at 100°C: (a) 8 h, (b) 24 h, (c) 48 h; and surface modified CTAB diatoms at (d) 8 h, (e) 24 h, (f) 48 h.

Table 1.2 Hydrothermal Conversion of TiO_2 in to $BaTiO_3$ as a function of reaction time at 100 ºC

Specimen Type[a]	*Reaction Time (h)*	*(110) $BaTiO_3$/ (101) TiO_2*[b]
DE	8	1.4
DE	24	10.9
DE	48	25.6
CTAB	8	1.8
CTAB	24	22.1
CTAB	48	80.7

[a]"DE" refers to the starting frustules obtained as diatomaceous earth. "CTAB refers to DE frustule specimens that were exposed to a hexadecyltrimethylammonium bromide (CTAB) surfactant-based dissolution/reprecipitation process[67] prior to reactive conversion into anatase TiO_2.
[b]Ratio of the areas of the most intense x-ray diffraction peaks for $BaTiO_3$ (the (110) peak) and TiO_2 (the (101) peak).

Further quantification of both the 48 h specimens was performed using the XRD patterns from the $BaTiO_3/TiO_2$ mixtures. This analysis was performed by calculating the intensity ratio and the area ratio of the (100) peak for the $BaTiO_3$ and the (101) peak for the TiO_2, since these peaks are in close proximity on the 2θ scale. Area ratio for the non-CTAB treated specimen revealed the amount of conversion to be less than 92.8%, respectively. While the CTAB-treated specimen achieved greater than 98.8 % conversion, based on area ratio.

The absence of distinct (200)-type and (002)-type peaks in the barium titanate diffraction pattern in Figure 1.9f indicated that the $BaTiO_3$ had formed predominantly as a cubic polymorph as opposed to the stable tetragonal phase (note: the hydrothermal formation of cubic $BaTiO_3$ at $\leq 150^oC$ has been reported by a number of authors[15,16,30,70]). Scherrer analysis of the diffraction peaks in Figure 1.9f yielded an average crystallite size of 63 nm for the fully-converted (CTAB-treated) $BaTiO_3$ frustules.

Scanning electron images of a fully-converted (48 h, 100^oC, CTAB-treated) $BaTiO_3$ frustule and a partially-converted (48 h, 100^oC, non-CTAB-treated) $BaTiO_3$ frustule are shown in Figures 1.10 a and b, respectively. The overall 3-D morphology of the starting frustules was preserved in the $BaTiO_3$-converted frustules. BET analysis of the completely-converted $BaTiO_3$ specimens yielded a specific surface area of 12.8 m^2/g, which was comparable to that for the titania replicas (11.3 m^2/g) from which such $BaTiO_3$ was derived.

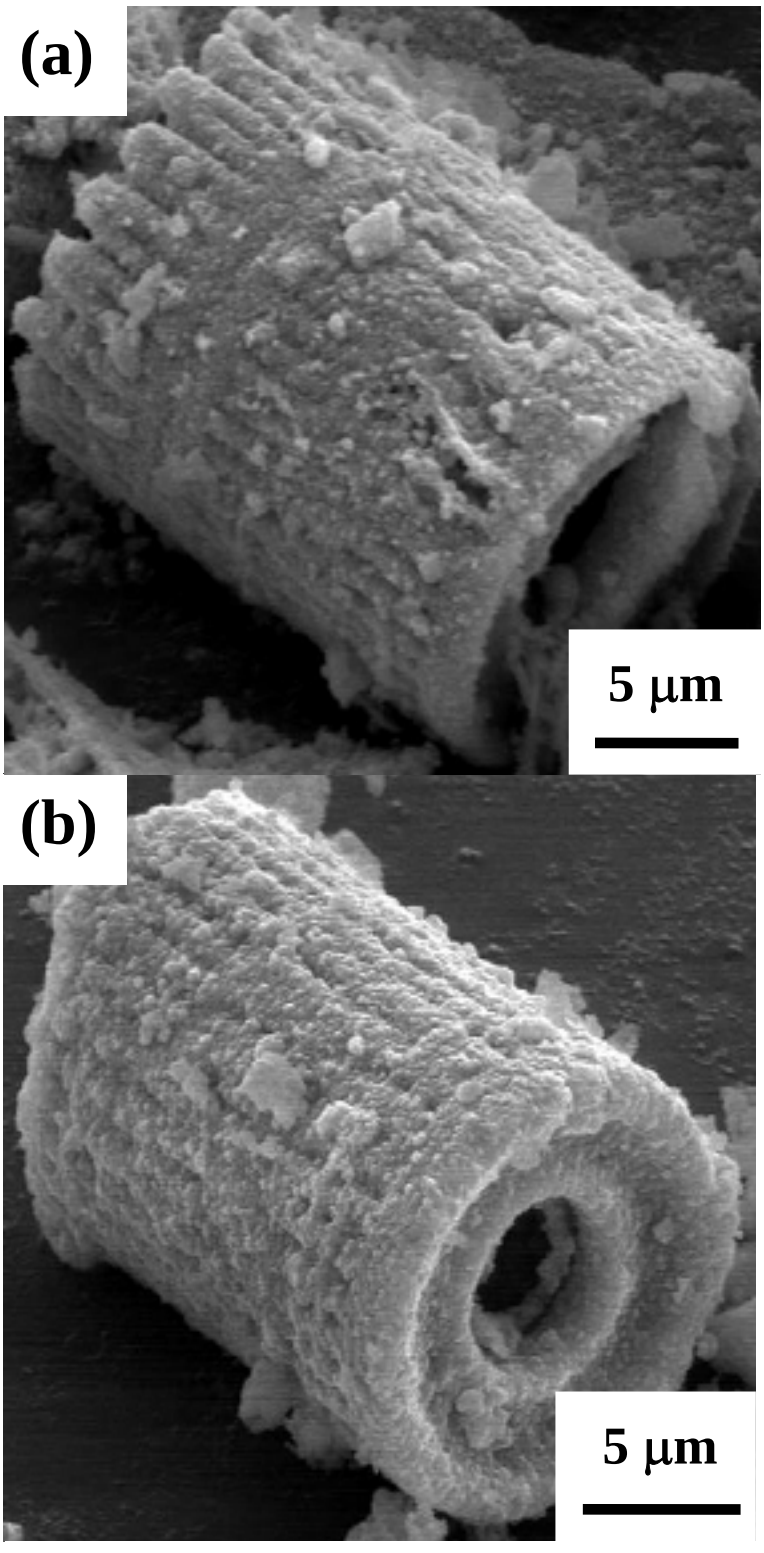

Figure 1.10 Secondary electron image of: (a) a CTAB-treated, TiO_2-converted microshell after hydrothermal conversion to $BaTiO_3$, (b) a non-CTAB-treated, TiO_2-converted microshell after hydrothermal conversion to $BaTiO_3$

The hydrothermal conversion of titania templates (e.g., microspheres, nanotubes) into barium titanate structures that retained the template shape has been reported by several authors.[15,71-73] Such shape preservation is consistent with so-called "*in-situ*" hydrothermal conversion, during which a conformal $BaTiO_3$ product layer is generated around the reacting TiO_2 template.[15,70,71,74] Hertl reported that such *in-situ* hydrothermal conversion of titania particles at 70-103°C was limited by the rate of reaction at the $TiO_2/BaTiO_3$ interface, when the barium hydroxide concentration in the aqueous solution exceeded 1M (as was the case in the present work).[74] The rate of hydrothermal conversion into $BaTiO_3$ via such an interfacial reaction-limited process should certainly have been enhanced with an increase in the starting surface area of the TiO_2 replicas, as was accomplished by starting with CTAB-treated silica frustule templates.

1.4 Conclusion

In conclusion, silica diatom frustules have been completely converted into nanocrystalline barium titanate structures, with a retention of the starting 3-D frustule morphology, through the use of a series of low-temperature fluid/solid reactions. Exposure of the frustules (obtained as DE) to a CTAB-bearing aqueous solution at 112°C resulted in a significant enhancement in the frustule surface area without an appreciable change in the 3-D microscale morphology. Subsequent reaction of the frustules with titanium tetrafluoride at 350°C for 2 h, and then with humid oxygen at 400°C for 5 h, yielded titania (anatase) frustule replicas. Hydrothermal reaction of the titania replicas with a barium hydroxide solution at 100°C for 48 h resulted in nearly complete conversion into nanocrystalline barium titanate structures that retained the 3-D

microscale frustule morphology. The enhanced surface area of the CTAB-treated frustules resulted in an increase in the specific surface area of the TiO_2 frustule replicas that, in turn, led in an increase in the rate of hydrothermal conversion into $BaTiO_3$ at 100^{o}C.

(This chapter was previously published as a short article in the Journal of Materials Research)[75]

1.5 References

1. G. H. Haertling: Ferroelectric ceramics: History and technology. *J. Am. Ceram. Soc.* **82**, 797 (1999).

2. C. Miclea, C. Tanasoiu, C. F. Miclea, and V. Tanasoiu: Advanced electroceramic materials for electrotechnical applications. *J. Optoelectron. Adv. Mater.* **4**, 51 (2002).

3. D. Pandey, A. P. Singh, and V. S. Tiwari: Developments in ferroelectric ceramics for capacitor applications. *Bull. Mater. Sci.* **15**, 391 (1992).

4. A. B. Alles, V. R. W. Amarakoon, and V. L. Burdick: Positive temperature coefficient of resistivity effect in undoped, atmospherically reduced barium titanate. *J. Am. Ceram. Soc.* **72**, 148 (1989).

5. A. C. Caballero, M. Villegas, J. F. Fernandez, M. Viviani, M. T. Buscaglia, and M. Leoni: Effect of humidity on the electrical response of porous $BaTiO_3$ ceramics. *J. Mater. Sci. Lett.* **18**, 1297 (1999).

6. A. Haeusler and J.-U. Meyer: A novel thick film conductive type CO_2 sensor. *Sens. Actuators B Chem.* **34**, 388 (1996).

7. J. Li, J. Yong, and M. Kuwabara: Photoluminescence and its enhancement of Pr^{+3}-doped $BaTiO_3$ phosphor. *Jpn. J. Appl. Phys. 2 Lett.* **44**, L708 (2005).

8. D. Hernandez Cruz, B. Sahouli, A. Tork, E. J. Knystautas, and R. A. Lessard: XPS and RBS analysis of the composition and structure of barium titanate thin films to be used in DRAMs. *SPIE Proc.* 4296, 244 (2001).

9. C. Pithan, D. Hennings, and R. Waser: Progress in the synthesis of nanocrystalline $BaTiO_3$ powders for MLCC. *Int. J. Appl. Ceram. Technol.* **2**, 1 (2005).

10. D. F. K. Hennings, B. Seriyati Schreinemacher, and H. Schreinemacher: Solid-state preparation of $BaTiO_3$-based dielectrics, using ultrafine raw materials. *J. Am. Ceram. Soc.* **84**, 2777 (2001).

11. H. S. Potdar, P. Singh, S. B. Deshpande, P. D. Godgole, and S. K. Date: Low-temperature synthesis of ultrafine barium titanate ($BaTiO_3$) using organometallic barium and titanium precursors. *Mater. Lett.* **10**, 112 (1990).

12. S. Wada, M. Narahara, T. Hoshina, H. Kakemoto, and T. Tsurumi: Preparation of nm-sized $BaTiO_3$ particles using a new 2-step thermal decomposition of barium titanyl oxalate. *J. Mater. Sci.* **38**, 2655 (2003).

13. S. O'Brien, L. Brus, and C. B. Murray: Synthesis of monodisperse nanoparticles of barium titanate: Toward a generalized strategy of oxide nanoparticle synthesis. *J. Am. Chem. Soc.* **123**, 12085 (2001).

14. M. P. Pechini: Method of preparing lead and alkaline earth titanates and niobates and coating methods using the same to form a capacitor. *U.S. Patent No. 3,330,697*, 1967.

15. M. Z.-C. Hu, V. Kurian, E. A. Payzant, C. J. Rawn, and R. D. Hunt: Wet-chemical synthesis of monodispersed barium titanate particles – hydrothermal conversion of TiO_2 microspheres to nanocrystalline $BaTiO_3$. *Powder Technol.* **110**, 2 (2000).

16. W. Zhu, S. A. Akbar, R. Asiaie, and P. K. Dutta: Synthesis, microstructure, and electrical properties of hydrothermally prepared ferroelectric $BaTiO_3$ thin films. *J. Electroceram.* **2**, 21 (1998).

17. R. Ueyama, M. Harada, T. Ueyama, T. Yamamoto, T. Shiosaki, K. Kiyoshi, K. Koumoto, and W. S. Seo: Preparation of $BaTiO_3$ ultrafine particles by micro-emulsion charring method. *J. Mater. Sci. Mater. Electron.* **11**, 139 (2000).

18. B. D. Stojanovic: Mechanochemical synthesis of ceramic powders with perovskite structure. *J. Mater. Process Technol.* **143-144**, 78 (2003).

19. S. Luo, Z. Tang, W. Yao, and Z. Zhang: Low-temperature combustion synthesis and characterization of nanosized tetragonal barium titanate powders. *Microelectron. Eng.* **66**, 147 (2003).

20. M. H. Frey and D. A. Payne: Nanocrystalline barium titanate: Evidence for the absence of ferroelectricity in sol-gel derived thin-layer capacitors. *Appl. Phys. Lett.* **63**, 2753 (1993).

21. Y. Kamigaki, T. Nagakari, and S. Nanbu: Ceramic capacitor from cubic $BaTiO_3$. *Jpn. Patent No. 08330179* Dec. 13, 1996.

22. J. Wang, H. Wan, and Q. Lin: Properties of a nanocrystalline barium titanate on silicon humidity sensor. *Meas. Sci. Technol.* **14**, 172 (2003).

23. J. Wang, B. Xu, G. Liu, J. Zhang and T. Zhang: Improvement of nanocrystalline $BaTiO_3$ humidity sensing properties. *Sens. Actuators B Chem.* **66**, 159 (2000).

24. Q. Wei, W. D. Luo, B. Liao, Y. Liu, and G. Wang: Giant capacitance effect and physical model of nanocrystalline CuO-$BaTiO_3$ semiconductor as a CO_2 gas sensor. *J. Appl. Phys.* **88**, 4818 (2000).

25. M. A. R. C. Alencar, G. S. Maciel, C. B. de Araujo, and A. Patra: Er^{+3}-doped $BaTiO_3$ nanocrystals for thermometry: Influence of nanoenvironment on the sensitivity of a fluorescence based temperature sensor. *Appl. Phys. Lett.* **84**, 4753 (2004).

26. U. A. Joshi, S. Yoon, S. Baik, and J. S. Lee: Surfactant-free hydrothermal synthesis of highly tetragonal barium titanate nanowires: A structural investigation. *J. Phys. Chem.* **110** 12249 (2006).

27. J. H. Wei, J. Shi, Z. Y. Liu, and J. B. Wang: Polymer-assisted synthesis of $BaTiO_3$ nanorods. *J. Mater. Sci.* **41**, 3127 (2006).

28. Y. Luo, I. Szafraniak, N. D. Zakharov, V. Nagarajan, M. Steinhart, R. B. Wehrspohn, J. H. Wendorff, R. Ramesh, and M. Alexe: Nanoshell tubes of ferroelectric lead zirconate titanate and barium titanate. *Appl. Phys. Lett.* **83**, 440 (2003).

29. H. Nakano and H. Nakamura: Preparation of hollow $BaTiO_3$ and anatase spheres by the layer-by-layer colloidal templating method. *J. Am. Ceram. Soc.* **89**, 1455 (2006).

30. J.-Y. Lee, S.-H. Hong, J.-H. Lee, Y. K. Lee, and J.-Y. Choi: Uniform coating of nanometer-scale $BaTiO_3$ layer on spherical Ni particles via hydrothermal conversion of Ti-hydroxide. *J. Am. Ceram. Soc.* **88**, 303 (2005).

31. J. Aizenberg, J. C. Weaver, M. S. Thanawala, V. C. Sundar, D. E. Morse, and P. Fratzl: Skeleton of *Euplectella sp.*: Structural hierarchy from the nanoscale to the macroscale. *Science* **309**, 275 (2005).

32. J. Aizenberg, A. Tkachenko, S. Weiner, L. Addadi, and G. Hendler: Calcitic microlenses as part of the photoreceptor system in brittlestars. *Nature* **412**, 819 (2001).

33. L. Addadi, D. Joester, F. Nudelman, and S. Weiner: Mollusk shell formation: A source of new concepts for understanding biomineralization processes. *Chem. A. Eur. J.* **12**, 980 (2006).

34. D. Schuler, and R. B. Frankel: Bacterial magnetosomes: Microbiology, biomineralization and biotechnological applications. *Appl. Microbiol. Biotechnol.* **52**, 464 (1999).

35. E. Bauerlein: Biomineralization of unicellular organisms: An unusual membrane biochemistry for the production of inorganic nano- and microstructures. *Angew. Chem. Int. Ed.* **42**, 614 (2003).

36. J. R. Young, S. A. Davis, P. R. Bown, and S. Mann: Coccolith ultrastructure and biomineralisation. *J. Struct. Biol.* **126**, 195 (1999).

37. J. R. Young, and K. Henriksen: Biomineralization within vesicles: The calcite of coccoliths. *Rev. Mineral. Geochem.* **54**, 189 (2003).

38. M. Hildebrand, and R. Wetherbee: Components and control of silicification in diatoms, in *Progress in Molecular and Subcellular Biology*, Vol. 33, edited by W. E. G. Muller (Springer-Verlag, Berlin, 2003), p. 11.

39. S. A. Crawford, M. J. Higgins, P. Mulvaney, and R. Wetherbee: Nanostructure of the diatom frustule as revealed by atomic force and scanning electron microscopy. *J. Phycol.* **37**, 543 (2001).

40. F. E. Round, R. M. Crawford, and D. G. Mann: *The diatoms: Biology and morphology of the genera* (Cambridge University Press, Cambridge, 1990).

41. D. G. Mann, and S. J. M. Droop: Biodiversity, biogeography, and conservation of diatoms. *Hydrobiol.* **336**, 19 (1996).

42. T. Lebeau, and J.-M. Robert: Diatom cultivation and biotechnologically relevant products. Part I: Cultivation at various length scales. *Appl. Microbiol. Biotechnol.* **60**, 612 (2003).

43. E. O. Duerr, A. Molnar, and V. Sato: Cultured microalgae as aquaculture feeds. *J. Mar. Biotechnol.* **7**, 65 (1998).

44. K. E. Apt, P. G. Kroth-Pancic, and A. R. Grossmann: Stable nuclear transformation of the diatom *Phaeodactylum tricornutum*. *Mol. Gen. Genomics* **252**, 572 (1999).

45. H. Fisher, I. Robl, M. Sumper, and N. Kröger: Targeting and covalent modification of cell wall and membrane proteins heterogeneously expressed in the diatom *Cylindrotheca fusiformis J. Phycol.* **35**, 113 (1999).

46. M. Hildebrand: Prospects of Manipulating Diatom Silica Nanostructure. *J. Nanosci. Nanotechnol. 5*, 146 (2005).

47. K. H. Sandhage, R. L. Snyder, G. Ahmad, S. M. Allan, Y. Cai, M. B. Dickerson, C. S. Gaddis, M. S. Haluska, S. Shian, M. R. Weatherspoon, R. A. Rapp, R. R. Unocic, F. M. Zalar, Y. Zhang, M. Hildebrand, and B. P. Palenik: Merging biological self-assembly with synthetic chemical tailoring: The potential for 3-D genetically-engineered micro/nanodevices (3-D GEMS). *Int. J. Appl. Ceram. Technol.*, **2**, 317 (2005).

48. K. H. Sandhage: Shaped microcomponents via reactive conversion of biologically-derived microtemplates. *U.S. Patent No. 7,067,104*, June 27, 2006.

49. K. H. Sandhage, M. B. Dickerson, P. M. Huseman, M. A. Caranna, J. D. Clifton, T. A. Bull, T. J. Heibel, W. R. Overton, and M. E. A. Schoenwaelder: Novel, bioclastic route to self-assembled, 3-D, chemically tailored meso/nanostructures: Shape-preserving reactive conversion of biosilica (diatom) microshells. *Adv. Mater.* **14**, 429 (2002).

50. F. M. Zalar, M. B. Dickerson, and K. H. Sandhage: Self-Assembled, 3-D Nanoparticle Structures with Tailored Chemistries via the BaSIC Process, in *Processing and Fabrication of Advanced Materials XI*, Vol. 2, edited by T. S. Srivatsan, R. A. Varin (ASM International, Materials Park, OH, 2003), p. 415

51. R. R. Unocic, F. M. Zalar, P. M. Sarosi, Y. Cai, and K. H. Sandhage: Anatase assemblies from algae: Coupling biological self-assembly of 3-D nanoparticle structures with synthetic reaction chemistry. *Chem. Commun.* [7] 795 (2004).

52. Y. Cai, S. M. Allan, F. M. Zalar, and K. H. Sandhage: Three-dimensional magnesia-based nanocrystal assemblies via low-temperature magnesiothermic reaction of diatom microshells. *J. Am. Ceram. Soc.* **88**, 2005 (2005).

53. S. Shian, Y. Cai, M. R. Weatherspoon, S. M. Allan, and K. H. Sandhage: Three-dimensional assemblies of zirconia nanocrystals via shape-preserving reactive conversion of diatom microshells. *J. Am. Ceram. Soc.* **89**, 694 (2006).

54. J. C. Lytle, H. Yan, R. T. Turgeon, and A. Stein: Multistep, low-temperature pseudomorphic transformations of nanostructured silica to titania via a titanium oxyfluoride intermediate. *Chem. Mater.* 16, 3829 (2004).

55. J. S. Machin, D. L. Deadmore: Thermal stability of titanium dioxide. *Nature* **189**, 223 (1961).

56. Y. Cai, M. R. Weatherspoon, E. Ernst, M. S. Haluska, R. L. Snyder, and K. H. Sandhage: 3-D microparticles of $BaTiO_3$ and Zn_2SiO_4 via the chemical (sol-gel, acetate, or hydrothermal) conversion of biological (diatom) templates. *Ceram. Eng. Sci. Proc.* **27**, 49 (2006).

57. M. W. Anderson, S. M. Holmes, N. Hanif, and C. S. Cundy: Hierarchical pore structures through diatom zeolitization. *Angew. Chem. Int. Ed.* **39**, 2707 (2000).

58. Y. Wang, Y. Tang, A. Dong, X. Wang, N. Ren, and Z. Gao: Zeolitization of diatomite to prepare hierarchical porous zeolite materials through a vapor phase transport process. *J. Mater. Chem.* **12**, 1812 (2002).

59. C. S. Gaddis and K. H. Sandhage: Freestanding microscale 3-D polymeric structures with biologically-derived shapes and nanoscale features. *J. Mater. Res*. **19**, 2541 (2004).

60. N. L. Rosi, C. S. Thaxton, and C. A. Mirkin: Control of nanoparticle assembly by using DNA-modified diatom templates. *Angew. Chem. Int. Ed.* **43**, 5500 (2004).

61. M. R. Weatherspoon, S. M. Allan, E. Hunt, Y. Cai, and K. H. Sandhage: Sol-gel synthesis on self-replicating single-cell scaffolds: Applying complex chemistries to nature's 3-D nanostructured templates. *Chem. Commun.* [5] 651 (2005).

62. Y. Cai and K. H. Sandhage: Zn_2SiO_4-coated microparticles with biologically-controlled 3-D shapes. *Phys. Stat. Sol. A* **202**, R105 (2005).

63. J. Zhao, C. S. Gaddis, Y. Cai, and K. H. Sandhage: Free-standing microscale structures of zirconia nanocrystals with biologically replicable 3-D shapes," *J. Mater. Res.* **20**, 282 (2005).

64. M. R. Weatherspoon, M. S. Haluska, Y. Cai, J. S. King, C. J. Summers, R. L. Snyder, and K. H. Sandhage: Phosphor microparticles of controlled 3-D shape from phytoplankton. *J. Electrochem. Soc.* **153**, H34 (2006).

65. C. S. Gaddis: *Diatom alchemy*. (M.S. thesis, Georgia Institute of Technology, 2004), p. 62.

66. S. Dudley, T. Kalem, and M. Akinc: Conversion of SiO_2 diatom frustules to $BaTiO_3$ and $SrTiO_3$. *J. Am. Ceram. Soc.* **89**, 2434 (2006).

67. C.E. Fowler, Y. Hoog, L. Vidal, and B. Lebeau: Mesoporosity in diatoms via surfactant induced silica rearrangement. *Chem. Phys. Lett.* **398,** 414 (2004).

68. E. P. Barrett-Joyner-Halenda, L. G. Joyner, and P. P. Halenda: The determination of pore volume and area distributions in porous substances. I. Computations from nitrogen isotherms. *J. Am. Chem. Soc.* **73**, 373 (1951).

69. B. D. Cullity and S. R. Stock: *Elements of X-Ray Diffraction 3rd Ed.* (Prentice Hall, New Jersey, 2001).

70. J.O. Eckert, Jr., C.C. Hung-Houston, B.L. Gersten, M.M. Lencka and R.E. Riman: Kinetics and mechanisms of hydrothermal synthesis of barium titanate. *J. Am. Ceram. Soc.* **79**, 2929 (1996).

71. K.-Y. Chen, and Y.-W. Chen: Preparation of monodispersed spherical barium titanate particles. *J. Mater. Sci.* **40**, 991 (2005).

72. N. P. Padture, and X. Wei: Hydrothermal synthesis of thin films of barium titanate ceramic nano-tubes at 200ºC. *J. Am. Ceram. Soc.* **86**, 2215 (2003).

73. K. Watanabe, T. Okada, I. Choe, Y. Sato: Organic vapor sensitivity in a porous silicon device. *Sensors and Actuators B*, **33**, 194-197 (1996).

74. W. Hertl: Kinetics of barium titanate synthesis. *J. Am. Ceram. Soc.* **71**, 879 (1988).

75. E. M. Ernst, B. C. Church, C. S. Gaddis, R. L. Snyder, K. H. Sandhage. Enhanced hydrothermal conversion of surfactant modified diatom microshells into barium titanate replicas. *J. Mate. Res.* **22,** 1121 (2007).

Chapter 2

Barium Strontium Titanate 3-D Replicas of Diatom Frustules

2.1 Introduction

Barium titanate (BT) is an attractive material in the electronics industry owing mainly to its ferroelectric properties. BT is only one compound that has the perovskite crystal structure which is capable of undergoing phase transitions at low temperatures to produce these properties. During the 1950's, Roy and his students expanded the application potential of BT by establishing a basis for multiple ion substitution for the A sites and B sites in the perovskite system.[1] One of the possible ion substitutions for BT is Sr^{2+} for Ba^{2+} in an A site to form barium strontium titanate (BST, $Ba_{1-X}Sr_XTiO_3$). This substitution is of interest because the stoichiometry of the product can be controlled for use in specific electronic applications such as tunable composite. As a derivative of BT, BST exhibits a Curie temperature. This temperature is dependent on the alkaline ratio of Ba:Sr. One of the most important Ba:Sr molar ratios is around 60:40, which Helmi *et al*. found to have a tetragonal to cubic transition around 6.3 ºC.[2] The Curie temperature is not the only property affected by the substitution. Zhou *et al*. found the dielectric constant to be 3 times higher than barium titanate.[3] This makes BST of great interest for applications which require switches,[4] tunable phase shifters,[5-8] capacitors for tunable radio frequency and microwave devices,[9-12] or dynamic random access memory.[13-15]

BST has been synthesized in many forms among which are thin films,[16] powders,[17-19] and nanotubes.[20] Although these structures are easily synthesized, a greater challenge lies in the ability to design 3-dimensional (3-D) shapes composed of BST with

complex morphologies. The only man-made structure of BST possessing a 3-D shape is a nanotube. Unfortunately, this is a simplistic structure and is limited by its shape. In contrast, nature provides complex 3-D structures from the skeletal frameworks of algae, referred to as diatoms, which possess fine features such as pores and channels. Figure 2.1 shows a secondary electron image of the diatom species *Aulacosira*. This type of diatom skeleton is commonly found in pool filtration media referred to as diatomaceous earth (DE). The skeletal structure is known as a frustule and is composed of amorphous silicon dioxide (SiO_2, silica). The frustules found in DE are not amorphous and are predominately cristobalite phase SiO_2, which is not very useful, but is ideal for conversion to other oxides. Previously, frustules of this type have been converted to other non-silica bearing structures using the patented BASIC (Bioclastic And Shape-preserving Inorganic Conversion)[21] process to form magnesium oxide (MgO),[22] titanium dioxide (TiO_2),[23] and zirconium oxide (ZrO_2).[24] A BST converted replica microshell could offer promise in electronic applications such as flexible antennas made of BST replica composite materials.

There are numerous methods which can be employed for processing BST depending on the desired morphology. In the 1950's Basmajian *et al*. and Kwestroo *et al*. generated BST powders by applying a solid state method similar to that used to make BT, in which $BaCO_3$, $SrCO_3$ and TiO_2 powders were mixed and sintered at 1350 to 1400 ºC.[25, 26] Unfortunately, this previous method requires ball milling, high temperature treatment, and cannot be employed for all applications. Phase shifters and microwave applications require thin films which, among other methods, can be deposited by radio frequency magnetron sputtering,[27] pulsed laser,[28, 29] or plasma jet[30] deposition and are not volatile to

the shape of the structure. Synthesis of titanates via aqueous solution or hydrothermal methods has gained attention due to lower synthesis temperatures and smaller particle size distribution. For example, Khollam *et al*. utilized a barium-strontium titanyl oxalate precursor in order to form $Ba_{0.75}Sr_{0.25}TiO_3$ powder.[31] Among other methods are catecholate,[32] sol-gel,[33, 34] acetate,[35] hydrothermal dissolution-precipitation,[18] and *in situ* hydrothermal.[36] The *in situ* hydrothermal method is the only process that has proven to preserve the shape of starting framework and, therefore, is the only method with potential to convert the 3-D microstructures of diatoms to BST.

The current research utilizes an *in situ* hydrothermal method at low temperature to produce replicas of diatom frustules which possess the same fine features but in a ferroelectric structure. After using a method to enhance the surface of the starting DE diatom frustules, DE was converted to TiO_2 microshell replicas using the method of Unocic *et al*.[23] The TiO_2 microshells were then subjected to a hydrothermal process to form BST microshell replicas. The conversions were performed over durations of 1 to 4 days and at temperatures of 100 and 200 ºC. Alkaline earth to titanium ratios were also examined for ratios of 4.18 to 16.70 at 100 ºC. The purpose of this research was to convert SiO_2 frustules to semiconducting replicas composed of BST.

2.2 Experimental Setup

2.2.1 CTAB Treatment of Diatomaceous Earth

Anticipating an increase in the amount of conversion with the starting specific surface area (SSA), the DE was pretreated using a method similar to that of Fowler *et al*.[37] to increase the SSA from 1.6 m^2/g to 197 m^2/g. 3.05 g of (1-

hexadecyl)trimethylammonium bromide (CTAB, 98% purity, Alfa Aesar, Ward Hill, MA) was introduced into a 30 mL aqueous solution of 700 mM NaOH (sodium hydroxide, Alfa Aesar) for 15 min followed by the addition of 5.0 g of DE. The solution was mixed for 15 min, and then transferred to a laboratory-fabricated cylindrical stainless steel (SS) vessel (2.4 cm I.D. × 15.2 cm L) and heat treated at 130 ºC for 72 h. After heat treatment, the treated DE was washed and filtered with 2.0 L of deionized (DI) water to dissolve the CTAB. Residual CTAB was removed during heat treatment at 1 ºC/min to 540 ºC followed by a 1 h isothermal hold.

The surfaces of the CTAB surface-modified frustules was studied using N_2 (nitrogen gas) adsorption at liquid nitrogen temperatures (-195.9 ºC) (Autosorb-1C, Quantachrome, Boyton, FL). The method of Brunauer-Emmett-Teller was used to calculate the SSA from the N_2 adsorption isotherm.[38] Figure 2.1 shows an secondary electron image of a CTAB-treated DE frustule. Unfortunately, the pore size (1.1 – 5.0 nm) affected by the treatment is distributed between the micropore (<2.0 nm) and mesoporous (2.0 – 5.0 nm) regimes and cannot be resolved by SEM. The increase in initial solution treatment temperature from 112 ºC to 130 ºC raised the SSA to 197 m^2/g. Based on the increased reaction with CTAB-treated frustules, experiments were performed using only CTAB-modified DE.

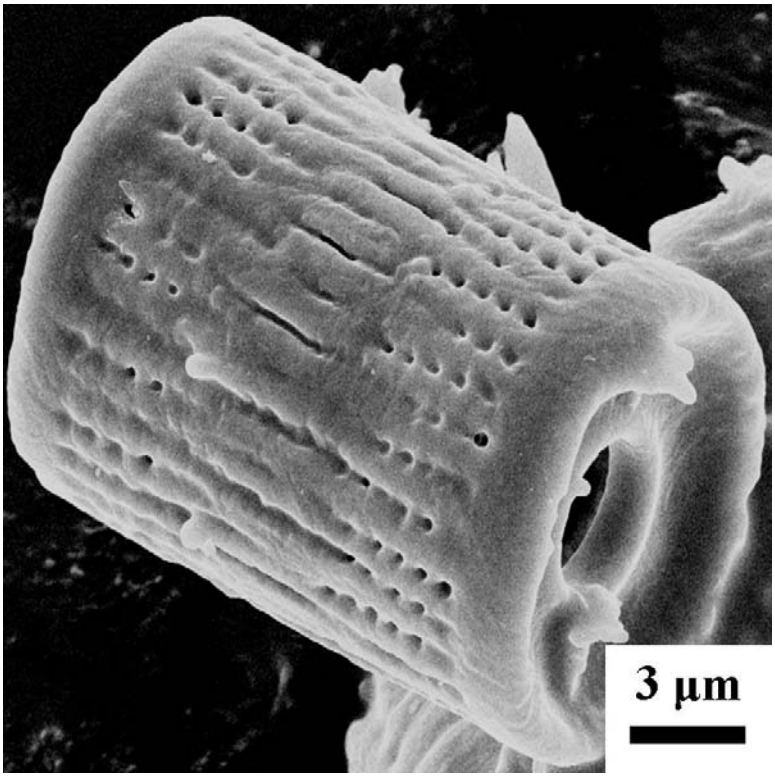

Figure 2.1 Secondary electron image of a CTAB-treated SiO_2 diatomaceous earth frustule.

2.2.2 Conversion of Frustules from SiO_2 into TiO_2 replicas

The CTAB-treated SiO_2 frustules were then converted to anatase TiO_2 replica microshells using a method similar to Unocic *et al*.[23] In an argon controlled environment, 200 mg of CTAB-modified DE was placed in a homemade nickel (Ni) tray. The Ni tray, in turn, was placed in a titanium (Ti) tube (2.54 cm D × 16.99 cm L, titanium tubing, Grade 2, McMaster-Carr, Atlanta, GA) containing 1.0 g of TiF_4 (titanium(IV) fluoride, Advanced Chemicals Research, Catoosa, OK) pre-weld sealed at one end. The opposite end of the tube was sealed by welding and the tube was heat treated at 5 ºC/min to 350 ºC and maintained for duration of 2 h. Following the heat treatment, the specimen was

removed from the tube and subjected to a second heat treatment in an irriguous, oxygen atmosphere formed by flowing oxygen at 1 L/min through 70 ºC water. The specimen was re-heated in a round MgO crucible (magnesium oxide, 2.54 cm D × 1.25 cm H, Ozark Technical Ceramics, Webb City, MO) at 5 ºC/min to 400 ºC and maintained for duration of 5 h. SEM analysis of a SiO_2 frustule after conversion to a TiO_2 exhibits exemplary preservation of the fine features such as pores, channels, and cylindrical shape (Figure 2.2). The main effect was the 95 % decrease in SSA, which cannot be resolved using SEM.

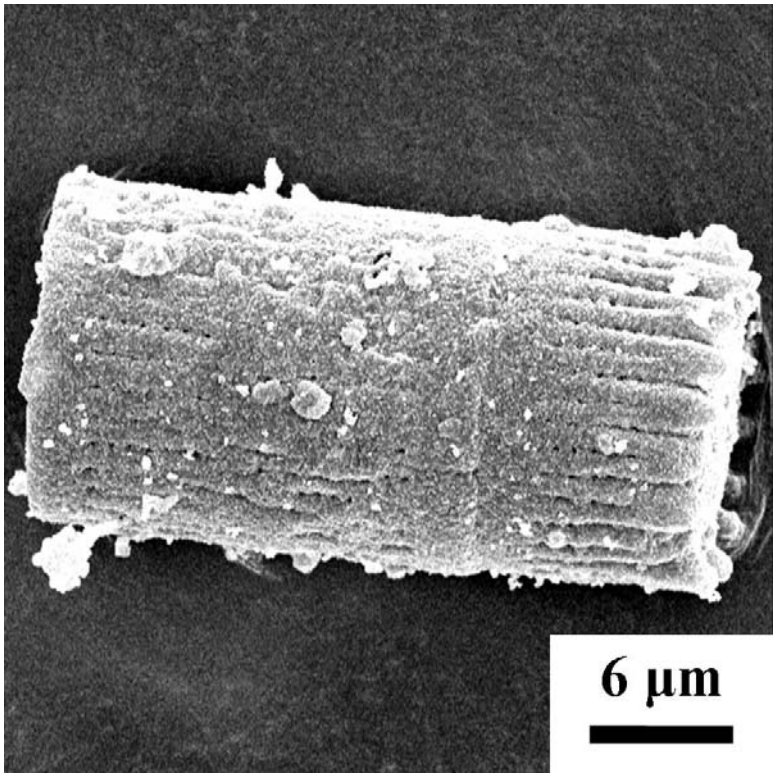

Figure 2.2 Secondary electron image of an SiO_2 diatomaceous earth frustule after conversion to TiO_2.

2.2.3 Hydrothermal Conversion of TiO_2 Microshells into $Ba_{1-X}Sr_XTiO_3$

Next, the TiO_2 microshells were converted to BST using an *in situ* hydrothermal reaction. 0.05 g of TiO_2 microshells were placed in a laboratory-fabricated PTFE liner (1.25 cm D × 3.95 cm L) with 1 mL of boiling distilled DI water. The liner was placed in a cylindrical, SS, laboratory-fabricated vessel (2.0 cm D × 8.3 cm L). The threads of the vessel were wrapped with PTFE sealant tape (1.25 cm W, Military Grade, McMaster-Carr) and loosely sealed. The vessel was then transferred to an argon controlled environment. Barium hydroxide octahydrate ($Ba(OH)_2 \cdot 8H_2O$, >98% purity, Alfa Aesar) was added to the tube in amounts ranging from 0.68 to 2.50 g. Strontium hydroxide octahydrate ($Sr(OH)_2 \cdot 8H_2O$, Alfa Aesar) was added during this period in amount ranging from 0.13 to 0.50 g. The vessel was sealed hand-tight, removed from the controlled environment, and sealed with a pipe wrench to maximum resistance.

The vessel was then placed into an oven preheated to either 100 or 200 ºC for durations of 1 to 4 days. After the heat treatment, the vessel was removed from the oven and allowed to cool. No weight change was detected in the vessel after treatment. The specimen was washed 6 times for 10 min in ≥ 85 ºC DI water and dissolved barium hydroxide was decanted at the end of each wash period. The specimen was dried for 24 h at 80 ºC.

The particle size and morphology of the converted frustules were examined by SEM (LEO-1530, Zeiss, Germany). Electron dispersive spectroscopy (EDS) was used to confirm the presences of Ba, Sr, and Ti. Phase identification was performed using X-ray diffraction (XRD) (Alpha-1, Cu-Kα radiation, Panalytical, Netherlands). Vegard's law was used to quantify the compositions of the specimens. An extensive literature search

was performed to locate a study in which a full spectrum of XRD patterns of compositions ranging from $BaTiO_3$ to $SrTiO_3$ were measured, but such a study was not found. Therefore, considering these perovskite systems possess similar structures which differ only in the size of the Group II cation, an attempt was made to calculate the alkaline % Sr (Sr/[Ba + Sr]) based on interpolation between the accepted patterns for $Ba_{1-X}Sr_XTiO_3$ (X = 0, 0.23, 0.4 0.6, 0.744, 1). Using the primary star patterns from the ICDD PDF-4+ 2006 database, lattice parameters and their respective alkaline % Sr, for the known $Ba_{1-X}Sr_XTiO_3$ compositions (Table 1), were plotted (Figure 2.3) to calculate the variation of lattice parameter with composition. The r^2 value for the Vegard's Law plot was >0.99. Hence, to calculate the composition of the present specimens the following equation was used:

$$\%\ Sr = \frac{a - 4.0045}{-0.1024} \times 100 \qquad \text{Eqn. 1}$$

Using an XRD pattern analysis program (*Jade 7 XRD Pattern Processing Identification & Quantification*), Scherrer analysis was performed to calculate the crystallite size from the full-width-at-half-maximum of the peaks in the XRD patterns. The surface characteristics of the microshells were examined using N_2 gas adsorption. Effects of post hydrothermal synthesis heat treatment were studied using TGA (thermogravimetric analysis, STA 449C, Netzsch, Burlington, MA).

Table 2.1 Lattice parameters of $Ba_{1-X}Sr_XTiO_3$, alkaline % Sr, and the alkaline % Sr calculated from the best-fit-line in the Vegard's law plot.

Lattice Parameter	*Alkaline % Sr*	*Calculated Alkaline % Sr*
4.009	0	-4.4
4.006	0	-1.5
3.977	23.0	26.9
3.965	40.0	38.6
3.947	50.0	56.2
3.925	74.4	77.6
3.905	100	97.2
3.903	100	99.1
3.901	100	101.0

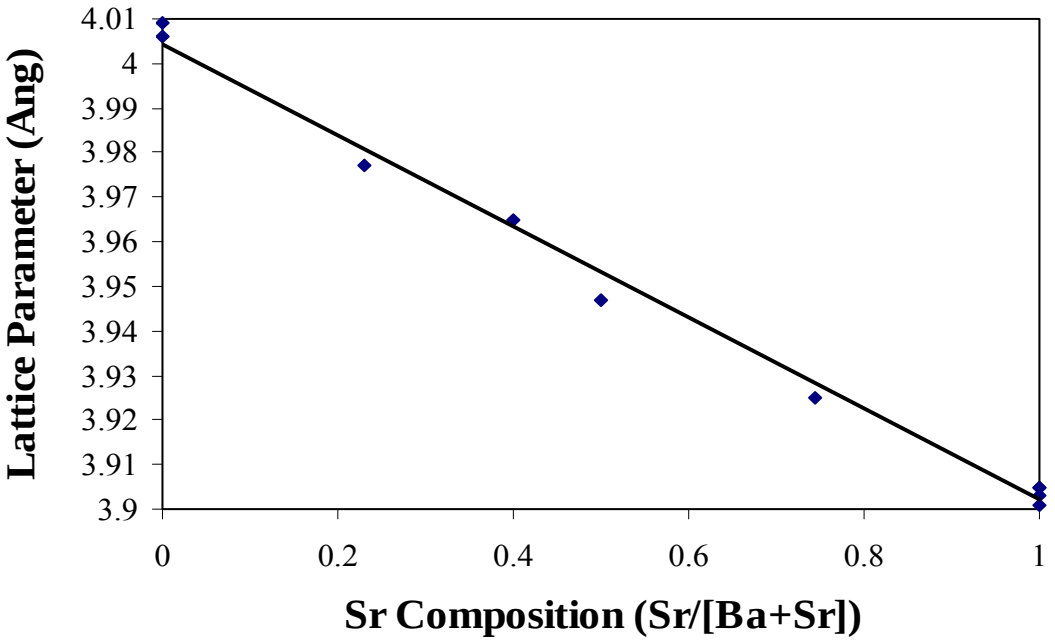

Figure 2.3 Vegard's Law Plot generated from the lattice parameters of the $Ba_{1-X}Sr_XTiO_3$ for X = {0, 0.23, 0.4, 0.6, 0.74, 1} with an ICDD Star quality mark, vs alkaline % of Sr.

2.3 Results and Discussion

XRD analysis was performed on each of the specimens between 20º and 60º 2θ. The diffractometer was calibrated using Si (silicon) standard (SRM 640a, >99.999 % purity, 2 μm average particle size, National Institute of Standards and Technology). The 0.006º 2θ shift in the standard pattern was compensated for in each experimental pattern. The specimens converted at 100 °C all exhibited BST peaks located within less than 0.05º 2θ of the accepted peaks for $Ba_{0.6}Sr_{0.4}TiO_3$. All the patterns were scaled to the height of the (110) peak, which is the most intense peak for the BST perovskite structures

in this study. Therefore, all comparisons are made using the information from the (110) BST peak and the dominant (101) peak of the anatase phase.

All the XRD patterns of the specimens exhibited only two phases; a cubic phase of BST and the anatase phase of TiO_2. In contrast to $BaTiO_3$, the cubic phase of BST has been reported to be the stable phase at room temperature.[20, 34, 36, 39, 40] The composition of the specimens was calculated from the Vegard's law plot (Figure 2.3). Using Eqn. 1, an average of 34.6 ± 2.9 alkaline % Sr was calculated for the 100 ºC specimens after 4 days of conversion. This may be an acceptable value for $Ba_{0.60}Sr_{0.40}TiO_3$ considering 38.6 ± 3.7 alkaline % Sr was calculated using Eqn. 1 and the accepted lattice parameter for $Ba_{0.60}Sr_{0.40}TiO_3$.[41]

Scherrer analysis of the patterns at 100 ºC indicated an increase in crystallite size with an increase in [Ba + Sr]/Ti. Figure 2.4 shows the patterns for the 100 ºC specimens after 24 h with [Ba + Sr]/Ti ratios of 4.18, 8.35, 16.70. The distribution of crystallite sizes ranged from 29.0 ± 4.3 nm, for the lowest [Ba + Sr]/Ti ratio (4.2), to 45.1 ± 5.6, for the highest [Ba + Sr]/Ti ratio (16.7). Only the region between 30.86° to 32.86° 2θ are shown so the narrowing of the peaks can be clearly observed.

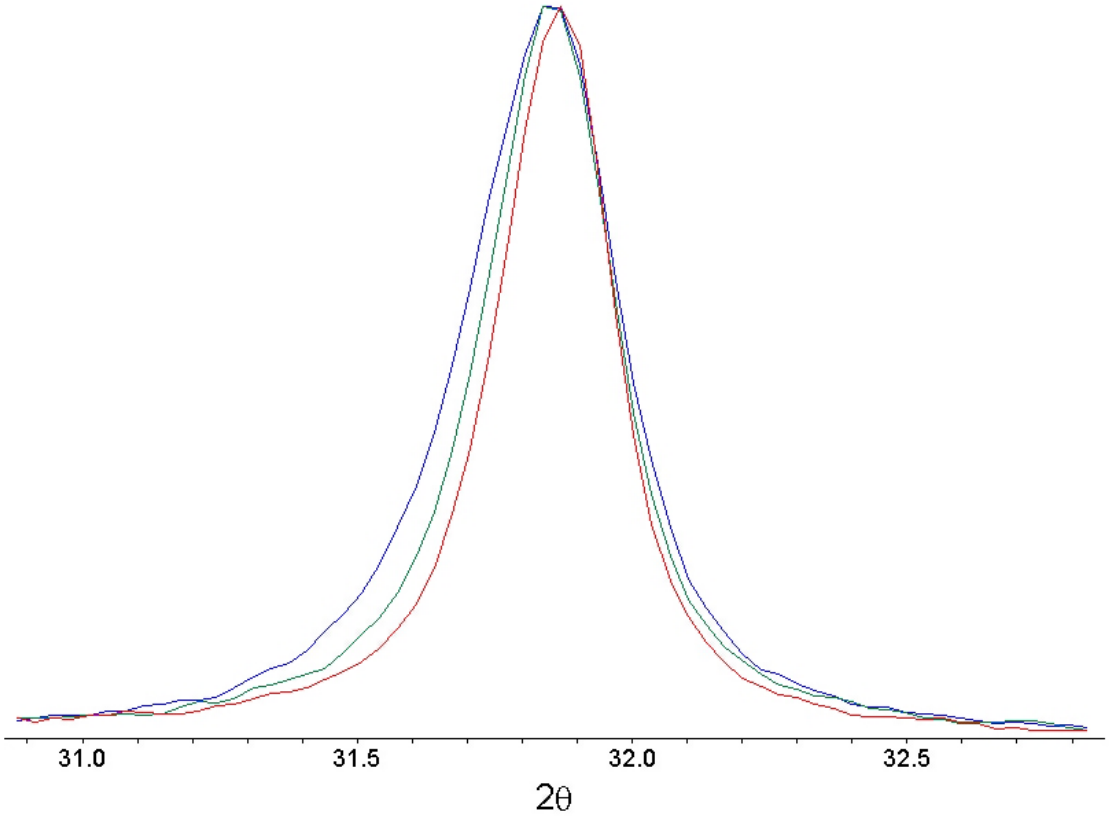

Figure 2.4 (110) peaks for $Ba_{0.6}Sr_{0.4}TiO_3$ after 24 h of conversion and atomic [Ba + Sr]/Ti ratio of 4.2 (blue), 8.4 (green), and 16.7 (red), after 24 h of conversion at 100 ºC.

Figures 2.5 – 2.7 compare the XRD patterns of the 100 °C specimens conducted over the periods of 1, 2 and 4 days, respectively, with an atomic Ba/Sr ratio of 4.52. The patterns were examined to determine the fraction converted as a function of time and atomic [Ba + Sr]/Ti ratio. The fraction of conversion of the 100 °C specimens, with the same Ba/Sr ratio, exhibited an increase with an increase in duration of heat treatment. Although the maximum amount of conversion was observed after 4 days, the difference from 2 to 4 days was minimal and the majority of conversion occurred within 2 days

(Table 2.2). Roeder and Slamovich reported similar results (finding the majority of reaction occurred after 2 days) although their specimens exhibited a biphasic split in the (110) peak after 1 day.[18]

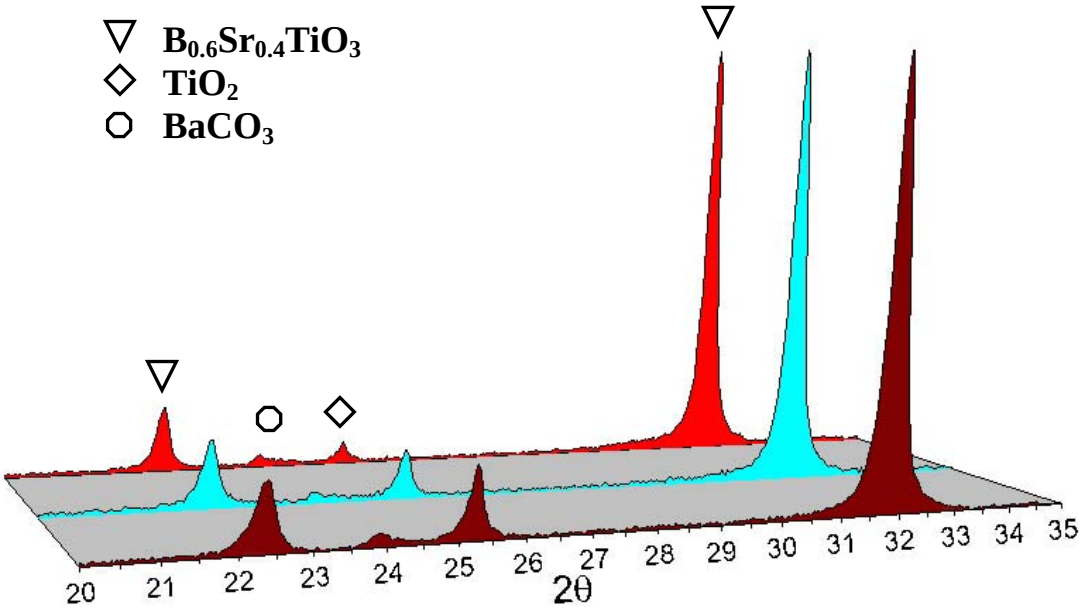

Figure 2.5 Comparison of 100 ºC specimens of BST after 24 hours of conversion in solution with atomic [Ba+Sr]/Ti ratios of 4.2, 8.4, 16.7. (Increasing [Ba+Sr]/Ti from front to back)

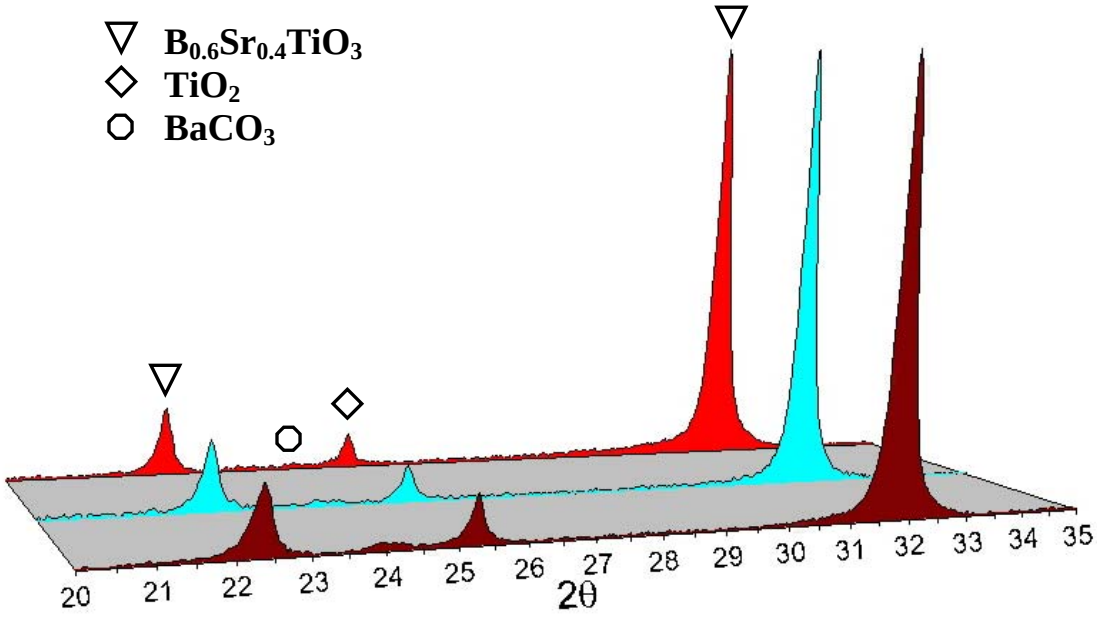

Figure 2.6 Comparison of 100 ºC specimens of BST after 2 days of conversion in solution with atomic [Ba+Sr]/Ti ratios of 4.2, 8.4, 16.7. (Increasing [Ba+Sr]/Ti from front to back)

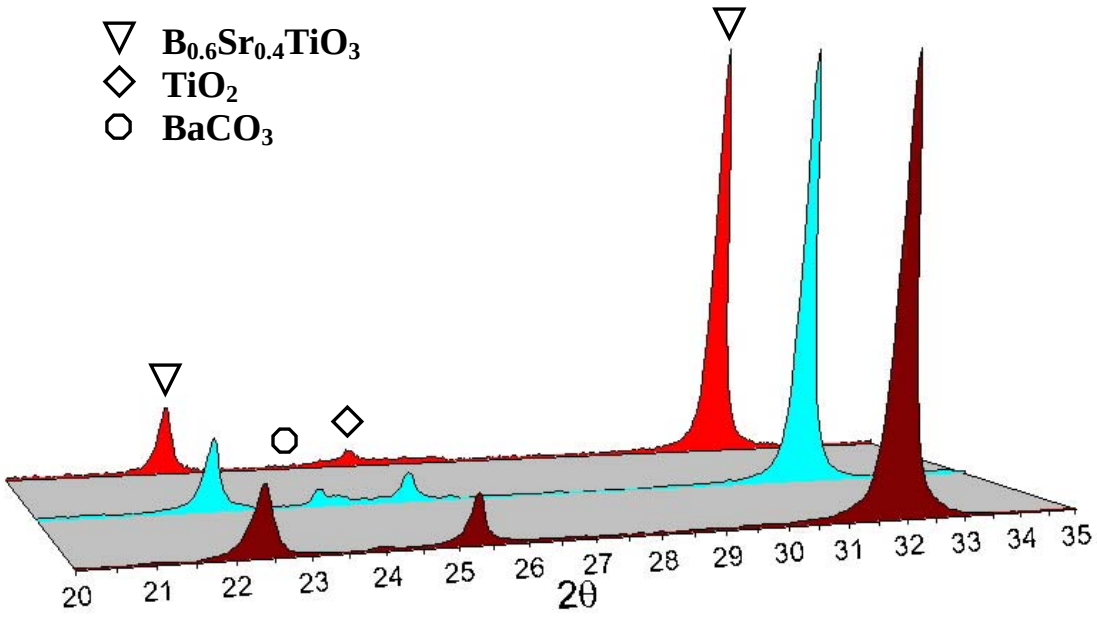

Figure 2.7 Comparison of 100 ºC specimens of BST after 4 days of conversion in solution with atomic [Ba+Sr]/Ti ratios of 4.2, 8.4, 16.7. (Increasing [Ba+Sr]/Ti from front to back)

Table 2.2 Ratios for the area of the (101) peak, for residual TiO_2, to the area of the (110) peak, for BST, in the XRD patterns for the 100 ºC specimens, spanning the time and the alkaline earth to titanium ratios.

Time (days)	*[Ba+Sr]/Ti = 4.2*	*[Ba+Sr]/Ti = 8.4*	*[Ba+Sr]/Ti = 16.7*
1	10.7	7.1	4.5
2	7.0	5.2	3.1
4	6.9	5.0	2.9

The conversions were attempted with atomic [Ba + Sr]/Ti ratios 4.18, 8.35 and 16.7. When the [Ba + Sr]/Ti was increased, the fraction converted was observed to increase for a constant reaction time. The greatest amount of conversion was observed for the specimens with a [Ba + Sr]/Ti ratio of 16.7. An investigation into the effect of heating and cooling rates was also performed on specimens at 100 °C over 4 day periods. Neither the heating nor the cooling rates were observed to have an effect on the amount of reaction. The main variables affecting the fraction of the frustules converted at 100 °C were reaction time and the atomic [Ba + Sr]/Ti ratio.

Figure 2.8a shows an SEM image of a frustule converted at 100 ºC for 4 days with a [Ba + Sr]/Ti ratio of 4.18. A higher resolution image of the frustule is also shown in Figure 8b. The frustule appears to have maintained the shape and fine features such as channels on the surface. The average particle size on the surface of this frustule was found to be 210 ± 40 nm by direct measurement of 100 particle diameters, parallel to the axis of the cylindrical structure.

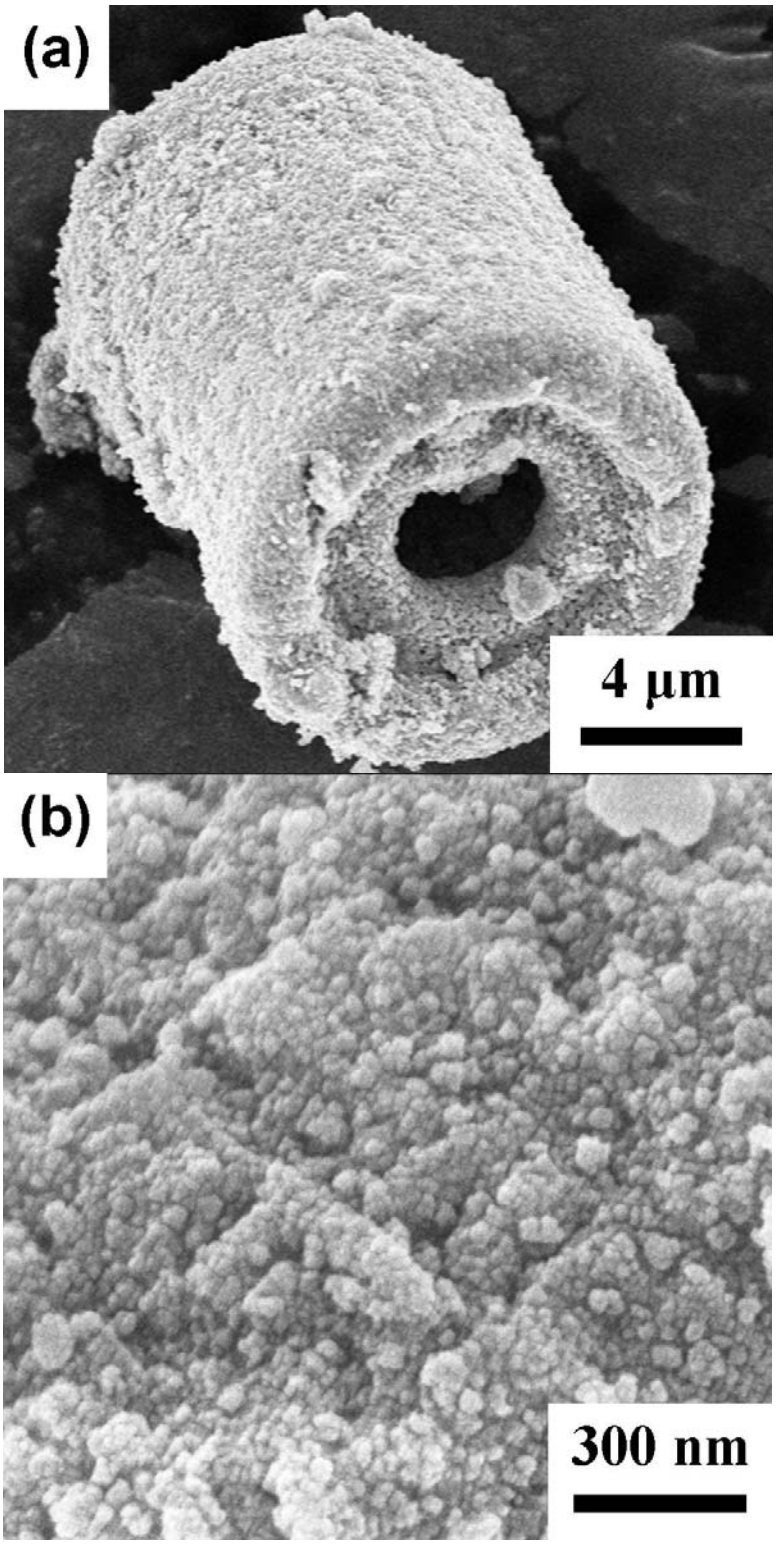

Figure 2.8 Secondary electron images of barium strontium titanate diatom converted at 100 ºC, with atomic ratio of [Ba + Sr]/Ti = 4.18: (a) replica frustule, (b) high resolution image of the particles on the surface of the replica.

Gas adsorption analysis was performed using N_2 (nitrogen gas) at liquid nitrogen temperature (-195.9 ºC) for all of the specimens with atomic [Ba + Sr]/Ti ratios of 4.18, 8.35, and 16.7. The method of Brunauer-Emmett-Teller was used to calculate the specific surface area (SSA).[38] Table 2.2 lists the [Ba + Sr]/Ti ratios and respective values for SSA. There were not enough [Ba + Sr]/Ti ratios studied to substantiate a correlation between SSA and [Ba + Sr]/Ti ratio. Hence, further investigation is needed to determine whether such a relationship exists.

Table 2.3 Values for [Ba + Sr]/Ti ratios and their corresponding SSA's

[Ba + Sr]/Ti	*SSA (m^2/g)*
4.18	3.5
8.35	2.8
16.70	1.9

Similar conversions were attempted at 200 °C with a Ba/Sr ratio of 4.52, the same times, and the same [Ba + Sr]/Ti ratios previously reported. Compared to the 100 ºC specimen reacted under the same conditions, the 200 ºC treatment yielded a greater amount of conversion (Figure 2.9). Examining the ratio of the area of the (101) peak for TiO_2 to the area of the (110) peak for BST, in the XRD pattern for the 200 ºC specimen, yielded a value of 0.6. When compared to the value of 2.9 for the 100 ºC specimen (Table 2.2), the 200 ºC specimen yielded a distinctly greater amount of conversion. This

increase in fraction converted was observed with the increase in the duration of heat treatment by examination of the (101) TiO_2 peak. The specimen XRD pattern shown in Figure 2.9b contained the greatest amount of conversion for all the parameters examined.

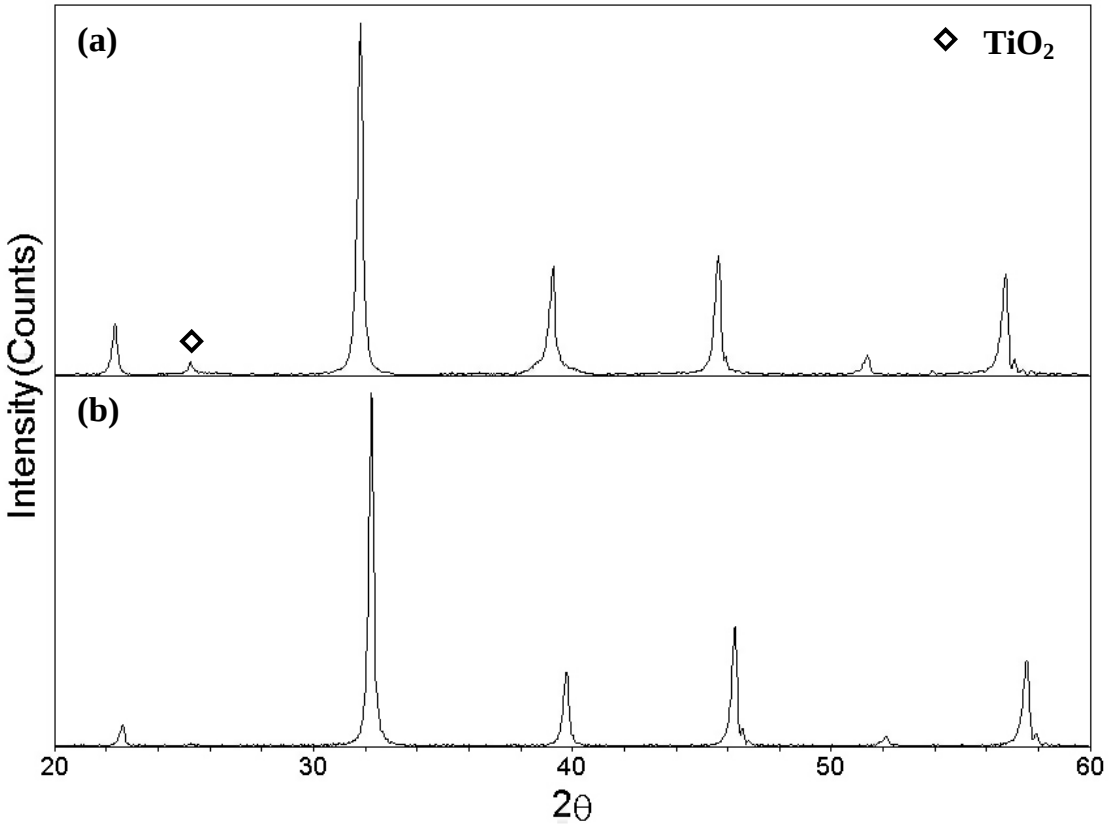

Figure 2.9 Comparison of the amount of conversion for the a) 100 ºC and b) 200 ºC treatments after 4 days of conversion in solution with [Ba+Sr]/Ti ratio of 16.7.

A result of increasing reaction temperature was a change in stoichiometry of the final product. Using the Vegard equation (Eqn. 1), the composition of the most reacted 200 ºC specimen after 4 days of reaction, with an atomic [Ba + Sr]/Ti ratio of 16.7, was calculated to be 82.1 ± 2.8 alkaline % Sr, (an incorporation of 137 % more Sr^{+2} into the

lattice with a 100 ºC increase in temperature). Figure 2.10 compares the peak positions of the (110) peaks from the XRD patterns of the 100 ºC and 200 ºC specimens. Vertical line markers for (110) peak positions of cubic phase $Ba_{0.6}Sr_{0.4}TiO_3$ and $SrTiO_3$ are also shown. Upon increasing the temperature from 100 ºC to 200 ºC, the peaks shifted due to the incorporation of the Sr^{+2} ions (despite having 4.52 times more Ba precursor than Sr precursor). A shift in the (110) peak with temperature was observed in all the 200 ºC specimens, and this shift was also observed to increase as a function of time. As with the amount of conversion, 97 % of the shifting occurred within 2 days.

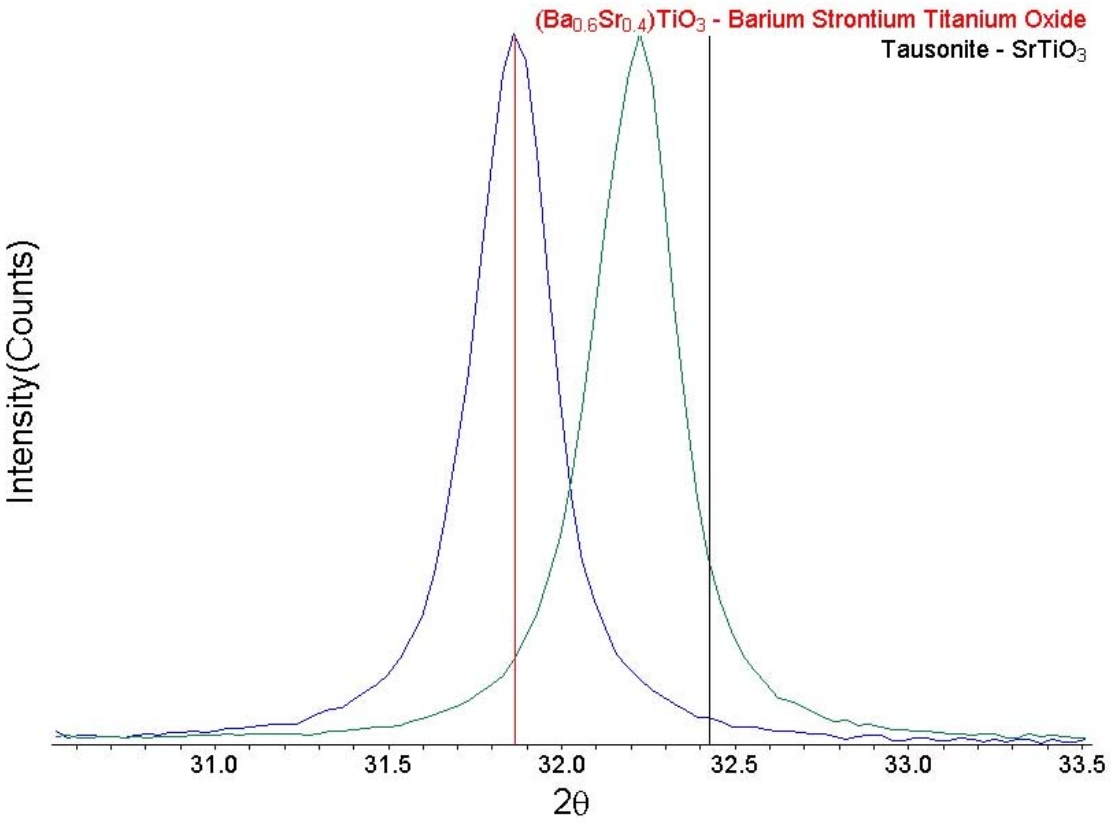

Figure 2.10 (110) peaks for $Ba_{1-X}Sr_XTiO_3$ after 4 days of conversion in solutions with [Ba+Sr]/Ti of 8.4, at (blue) 100 ºC and (green) 200 ºC.

A microshell after 4 days of conversion at 200 ºC with [Ba + Sr]/Ti of 16.7 and Ba/Sr of 4.52 is shown in Figure 2.11. This image confirms preservation of the shape and fine features, despite multiple conversions and the relatively high hydrothermal temperature used. An average particle size of 94 ± 23 nm was calculated from high resolution images (using the same conditions discussed for the 100 ºC specimen). This particle size is less than half the size measured for the microshells converted at 100 ºC. Calculations made from curve fitting the XRD patterns found the specimens synthesized at 200 ºC possessed an average crystallite size of 68.6 ± 4.3 nm in contrast to the 100 ºC specimens which possessed an average crystallite size of 113.3 ± 12.9 nm. This is possibly due to faster reaction kinetics at higher temperature, causing more sites to become active on the surface of the microshell.

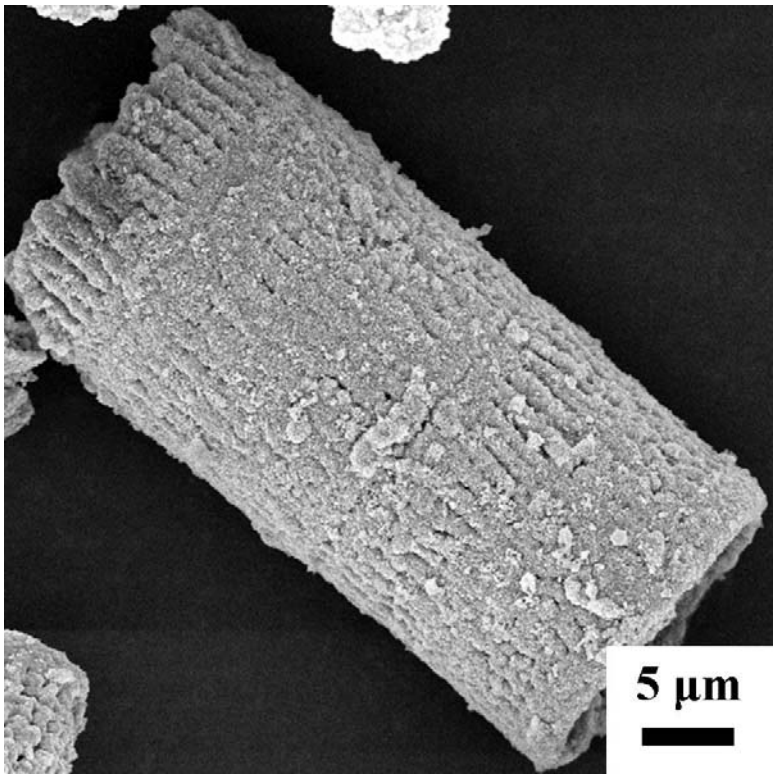

Figure 2.11 SEM photograph of a BST frustule after 4 days at 200 ºC, [Ba+Sr]/Ti = 16.7, Ba:Sr = 4.52

TGA was performed on a 100 ºC specimen converted over a 2 day period with contained a [Ba + Sr]/Ti ratio of 16.7. The heat treatment was performed at a ramp rate of 10 ºC/min to 1000 ºC and held for 2 hrs. There was a mass loss of 3.54 % which, in $BaTiO_3$, has been attributed to desorption of physisorbed water and OH^- ions trapped in oxygen vacancies at temperatures below 500 ºC and decomposition of carbonates above this temperature.[42-47] Heat treatment failed to affect the tetragonality of the structure and did not result in the formation of other intermediate BST phases.

2.4 Conclusion

In conclusion, this research demonstrates the nearly complete conversion of silica diatom frustules to barium strontium titanate with preservation of the frustule and shape through the use of low-temperature in-situ fluid/solid reactions. DE was treated with CTAB to increase the SSA, and hence, increase the number of reaction sites. A secondary conversion via a chemical vapor reaction with the titanium(IV) fluoride at 350 ºC for 2 h, followed by exposure to humid oxygen at 400 ºC for 5 h, produced anatase titania frustules. Further hydrothermal reactions using Ba and Sr hydroxide bearing precursors were used to convert the titania to cubic forms of $Ba_XSr_{1-X}TiO_3$ of varying molar compositions depending on temperature and time. It was found that the amount of Sr substituted into the A-sites in the perovskite structure increased with reaction time and temperature. The amount of conversion was found to depend on reaction time and the atomic [Ba + Sr]/Ti composition of the starting precursors (increasing conversion observed with increases in alkaline earth content).

2.5 References

1. R. Roy: Multiple ion substitution in the perovskite lattice. *Journal of the American Ceramic Society*. **37,** 581 (1954).

2. H. Abdelkefi, H. Khemakhem, G. Velu, J. C. Carru and R. V. d. Muhll: Dielectric properties and ferroelectric phase transitions in $Ba_XSr_{1-X}TiO_3$ solid solution. *Journal of Alloys and Compounds*. **399,** 1 (2005).

3. L. Zhou, P. M. Vilarinho and J. L. Baptista: Dependence of the structural and dielectric properties of $Ba_{1-X}Sr_xTiO_3$ ceramic solid solutions on raw material. *Journal of the European Ceramic Society*. **19,** 2015 (1999).

4. G. Subramanyam, F. Ahamed, R. Biggers and A. Campbell: Design considerations for a novel coplanar waveguide based ferroelectric varactor shunt switch. *Integrated Ferroelectrics*. **77,** 207 (2005).

5. S. B. Majumder, M. Jain, R. S. Katiyar, F. W. Keuls and F. A. Miranda: Sol-gel derived grain oriented barium strontium titanate thin films for phase shifter applications. *Journal of Applied Physics*. **90,** 896 (2001).

6. F. Zimmermann, M. Voigts, C. Weil, R. Jakoby, P. Wang, W. Menesklou and E. Ivers-Tiffee: Investigation of barium strontium titanate thick films for tunable phase shifters. *Journal of the European Ceramic Society*. **21,** 2019 (2001).

7. H.-S. Kim, T.-S. Hyun, H.-G. Kim, I.-D. Kim, T.-S. Yun and J.-C. Lee: Orientation effect on microwave dielectric properties of Si-integrated Ba0.6Sr0.4TiO3 thin films for frequency agile devices. *Applied Physics Letters*. **89,** 052902/1 (2006).

8. X. Wang, W. Lu, J. Liu, F. Liang and D. Zhou: Influence of MgO on structure and low-frequency properties of Ba0.6Sr0.4TiO3 ferroelectric ceramics. *Guisuanyan Xuebao*. **32,** 738 (2004).

9. N. K. Pervez, P. J. Hansen and R. A. York: High tunability barium strontium titanate thin films for rf circuit applications. *Journal of Applied Physics*. **85,** 4451 (2004).

10. A. Tombak, J. P. Maria, F. Ayguavives, J. Zhang, G. T. Stauf, A. I. Kingon and A. Mortazawi: Tunable barium strontium titanate thin film capacitors for RF and microwave applications. *IEEE Microwave Compon. Lett.* **12,** 2 (2002).

11. B. Su, J. E. Holmes, C. Meggs and T. W. Button: Dielectric and microwave properties of barium strontium titanate (BST) thick films on alumina substrates. *Journal of the European Ceramic Society*. **23,** 2699 (2003).

12. P. M. Suherman, T. J. Jackson, Y. Y. Tse, I. P. Jones, R. I. Chakalova, M. J. Lancaster and A. Porch: Microwave properties of Ba0.5Sr0.5TiO3 thin film coplanar phase shifters. *Journal of Applied Physics*. **99,** 104101/1 (2006).

13. A. Kumar and S. G. Manavalan: Characterization of barium strontium titanate thin films for tunable microwave and DRAM applications. *Surface and Coatings Technology*. **198,** 406 (2005).

14. M. Nayak, S. Ezhilvalavan and T. Y. Tseng: High-permittivity (Ba,Sr)TiO3 thin films. *Handbook of Thin Film Materials*. **3,** 99 (2002).

15. Y.-H. Xie, Y.-Y. Lin and T.-A. Tang: Characteristics of BST Thin Film Prepared by Novel Chemical Solution Deposition Method for High-Density DRAM Application. *Integrated Ferroelectrics*. **47,** 113 (2002).

16. S. C. Stowell, Y. Zhu, X. Zhang, S. Sengupta, L. C. Sengupta and A. J. Hsieh: Investigation of the effects of milling ceramic targets on the optical and electrical properties of BST thin films deposited by radiofrequency sputtering. *Integrated Ferroelectrics*. **21,** 441 (1998).

17. S. Komarneni, Q. Li, K. M. Stefansson and R. Roy: Microwave-hydrothermal processing for synthesis of electroceramic powders. *Journal of Materials Research*. **8,** 3176 (1993).

18. R. K. Roeder and E. B. Slamovich: Stoichiometry control and phase selection in hydrothermally derived $Ba_{1-X}Sr_XTiO_3$ powders. *Journal of the American Ceramic Society*. **82,** 1665 (1999).

19. H. Y. Tian, W. G. Luo, X. H. Pu, X. Y. He, P. S. Qiu and A. L. Ding: Synthesis and dielectric characteristic of Ba1-xSrxTiO3 thin films-based strontium-barium alkoxides derivatives. *Materials Chemistry and Physics*. **69,** 166 (2001).

20. X. Wei, A. L. Vasiliev and N. P. Padture: Nanotubes patterned thin films of barium-strontium titanate. *Journal of Materials Research*. **20,** 2140 (2005).

21. K. H. Sandhage: Shape microcomponents via reactive conversion of biologically-derived microtemplates. *U.S. Patent No. 7,067,104*, June 27, 2006.

22. K. H. Sandhage, M. B. Dickerson, P. M. Huseman, M. A. Caranna, J. D. Clifton, T. A. Bull, T. J. Heibel, W. R. Overton and M. E. A. Schoenwaelder: Novel, bioclastic route to self-assembled, 3D, chemically tailored meso/nanostructures: shape-preserving reactive conversion of biosilica (diatom) microshells. *Advanced Materials (Weinheim, Germany)*. **14,** 429 (2002).

23. R. R. Unocic, F. M. Zalar, P. M. Sarosi, Y. Cai and K. H. Sandhage: Anatase assemblies from algae: Coupling biological self-assembly of 3-D nanoparticle structures with synthetic reaction chemistry. *Chemical Communications*. **7,** 795 (2004).

24. S. Shian, Y. Cai, M. R. Weatherspoon, S. M. Allan and K. H. Sandhage: Three-dimensional assemblies of zirconia nanocrystals via shape-preserving reactive conversion of diatom microshells. *Journal of the American Ceramic Society*. **89,** 694 (2006).

25. J. A. Basmajian and R. C. DeVries: Phase Equilibria in the System $BaTiO_3$ - $SrTiO_3$. *Journal of the American Ceramic Society*. **40,** 373 (1957).

26. W. Kwestroo and H. A. M. Paping: The systems BaO-SrO-TiO_2, BaO-CaO-TiO_2, and SrO-CaO-TiO_2. *Journal of the American Ceramic Society*. **42,** 292 (1959).

27. H. Chen, C. Yang, C. Fu, L. Zhao and Z. Gao: The size effect of Ba0..6Sr0..4TiO3 thin films on the ferroelectric properties. *Applied Surface Science*. **252,** 4171 (2006).

28. D. Popovici, M. Noda, M. Okuyama, Y. Sasaki and M. Komaru: A low-loss BST thin film on initial nucleation layer for micro and millimeter wave tunable phase shifter. *Journal of the European Ceramic Society*. **26,** 1879 (2006).

29. W.-J. Kim, S. S. Kim, T. K. Song, S. E. Moon, E. K. Kim, S. J. Lee, M. H. Kwak, K. Y. Kang, W. Chang, S. W. Kircheofer, S. D. Qadri, J. M. Pond and J. S. Horwitz: Structure of ferroelectric (Ba,Sr)TiO3 thin films for tunable microwave devices. *Integrated Ferroelectrics*. **66,** 321 (2004).

30. Z. Bryknar, Z. Potucek, Z. Hubicka and J. Olejnicek: Luminescence properties of BaxSr1-xTiO3 thin films deposited by RF hollow cathode plasma jet system. *Ferroelectrics*. **335,** 95 (2006).

31. Y. B. Khollam, S. V. Bhoraskar, S. B. Deshpande, H. S. Potdar, N. R. Pavaskar, S. R. Sainkar and S. K. Date: Simple chemical route for the quantitative precipitation of barium-strontium titanyl oxalate precursor leading to $Ba_{1-X}Sr_XTiO_3$ powders. *Materials Letters*. **57,** 1871 (2003).

32. N. J. Ali and S. J. Milne: Synthesis and Processing characteristics of $Ba_{0.65}Sr_{0.35}TiO_3$ Powders from Catecholate Precursors. *Journal of the American Ceramic Society*. **76,** 2321 (1993).

33. H. P. Beck, W. Eiser and R. Haberkorn: Pitfalls in the synthesis of nanoscaled perovskite type compounds. Part II: Influence of different sol-gel preparation methods and characterization of nanoscaled mixed crystals of the type $Ba_{1-X}Sr_XTiO_3$ ($0 =< X =< 1$). *Journal of the European Ceramic Society*. **21,** 2319 (2001).

34. X. Xie, Y. Dong, C. Chen and L. Lin: Nonhydrolytic sol-gel synthesis of $Ba_{1-X}Sr_XTiO_3$ nanopowder. *Industrial & Engineering Chemistry Research*. **44,** 881 (2005).

35. I. P. Selvam and V. Kumar: Synthesis of nanopowders of $(Ba_{1-X}Sr_X)TiO_3$. *Materials Letters*. **56,** 1089 (2002).

36. M. H. Um and H. Kumazawa: Hydrothermal Synthesis of Ferroelectric barium and strontium titanate extremely fine particles. *J. Mater. Sci.* **35,** 1295 (2000).

37. C. E. Fowler, Y. Hoog, L. Vidal and B. Lebeau: Mesopososity in diatoms via surfactant induced silica rearrangment. *Chemical Physics Letters*. **398,** 414 (2004).

38. S. Brunauer, P. H. Emmett and E. Teller: Adorption of Gases in Multimolecular Layers. *Journal of the American Ceramic Society*. **60,** 309 (1938).

39. Y. B. Khollam, S. B. Deshpande, H. S. Potdar, S. V. Bhorasker, S. R. Sainkar and S. K. Date: Simple oxalate route for the preparation of barium-strontium titanate: $Ba_{1-X}Sr_XTiO_3$ powders. *Mater. Charact.* **53,** 63 (2005).

40. A. Ries, A. Z. Simoes, M. Cilense, M. A. Zaghete and J. A. Varela: Barium strontium titanate powder by polymeric precursor method. *Mater. Charact.* **50,** 217 (2003).

41. L. Keller et al., North Dakota State University, North Dakota, USA. ICDD Grant-in-Aid (1982).

42. B. D. Begg, E. R. Vance and J. Nowotny: Effect of Particle Size on the Room-Temperature Crystal Structure of Barium Titanate. *Journal of the American Ceramic Society*. **77,** 3186 (1996).

43. B. L. Newalker, S. Komarnemi and H. Katsuki: Microwave-hydrothermal synthesis and characterization of barium titanate powders. *Materials research Bulletin*. **36,** 2347 (2001).

44. H. S. Potdar, S. B. Deshpande and S. K. Date: Chemical coprecipitation of mixed (Ba + Ti) oxalates presursor leading to $BaTiO_3$ Powders. *Materials Chemistry and Physics*. **58,** 121 (1999).

45. E. Ciftci and M. N. Rahaman: Hydrothermal precipitation and characteriziation of nanocrystalline $BaTiO_3$ particles. *Journal of Materials Research*. **36,** 4875 (2001).

46. D. Hennings and S. Schreinemacher: Characterization of Hydrothermal Barium Titanate. *Journal of the European Ceramic Society*. **9,** 41 (1992).

47. R. Asiaie, W. Zhu, S. A. Akbar and P. K. Dutta: Characterization of Submicron Particles of Tetragonal $BaTiO_3$. *Chemistry of Materials*. **8,** 226 (1996).

Chapter 3

Microwave Assisted Hydrothermal Synthesis of Barium Titanate Algae Frustule Replicas

3.1 Introduction

Barium titanate ($BaTiO_3$) is one of the most widely used ferroelectric ceramics in the electro-ceramics industry. Its crystal structure exhibits a cubic to tetragonal phase transition when cooled below its Curie temperature around 120 ºC.[1] This phase transition induces dipoles which endow the material with attractive ferroelectric properties, such as higher dielectric constant, lower dielectric loss, and positive temperature coefficient of resistivity. Among electrical materials, these attributes make $BaTiO_3$ an attractive material for multilayer ceramic capacitors,[2-5] PTC resistors and thermistors,[6-11] and piezoelectric transducers.[12-14]

Extensive research has been conducted to create barium titanate in different forms, such as powders,[15-18] thin films,[19-22] nanoribbons,[23] nanorods,[24, 25] nanospheres,[26-29] nanotubes,[30-32] and nanowires.[33-35] During the 1950's, $BaTiO_3$ was primarily synthesized using solid state reaction methods, such as that of Rase and Roy[36, 37] involving the reaction of barium carbonate ($BaCO_3$) and titanium dioxide (TiO_2). The problem with this is the requirement of high temperature, which causes excessive grain growth. In recent years, alternative processes, such as aqueous solution methods, involving citrates,[38] oxalates,[39, 40] alkoxides,[14, 41] have been discovered which require lower temperatures . Two competing hydrothermal methods are the dissolution/precipitation method[42-44] and the in situ method.[45-48] The

dissolution/precipitation method requires the precipitation of barium and titanium salts out of solution, therefore, only spheres or other polyhedra are formed. Contrary to the dissolution of both precursors, in situ reactions form structures based one the shape of a solid precursor. Padture and Wei demonstrated the first shape preserving conversion of TiO_2 nanotubes to form $BaTiO_3$ in a basic solution of $Ba(OH)_2$.[31] Recently, low temperature hydrothermal reactions have been coupled with accelerated heating by microwave radiation.[49-51] Unfortunately, a review of the literature on $BaTiO_3$ synthesis revealed no attempts to combine the in situ hydrothermal method with microwave heating in order to convert solid TiO_2 to $BaTiO_3$ in an aqueous suspension of $Ba(OH)_2$.

Nanotubes, exhibit cylindrical shape preservation throughout $BaTiO_3$ conversion and, until recently, were the only 3-dimensional (3-D) shapes converted to $BaTiO_3$. Therefore, an in situ hydrothermal conversion should be viable for conversion of complex 3-D shapes on an industrial scale. Combined with microwave heating, this method is a clear solution to large-scale production of 3-D perovskite materials.

In contrast, nature is capable of assembling complex shapes from silicon dioxide (SiO_2, silica) based materials with sizes spanning the nano- and microscales. One attraction to SiO_2 based materials is the ability to convert them to other metal oxides. Previously, diatom frustules have been converted to other non-silica bearing structures via the patented BASIC (Bioclastic And Shape-preserving Inorganic Conversion) gas/silica displacement process.[52-57] Reactive conversion of SiO_2 diatom frustules to $BaTiO_3$ via the BaSIC process, followed by an in-situ hydrothermal conversion, was previously discussed in the paper by Ernst *et al*.[58] Using a method similar to that of Fowler *et al*.[59], the SiO_2 precursor frustules were surface modified to increase the specific

surface area (SSA) from 1.6 m^2/g to >100 m^2/g. This SSA increase was found to increase the amount of hydrothermal $BaTiO_3$ conversion, yielding nearly phase pure $BaTiO_3$.

In the present research, SiO_2 diatomaceous earth (DE) was modified to increase the SSA of the frustules using (1-hexadecyl)trimethylammonium bromide (CTAB, $CH_3(CH_2)_{15}N(CH_3)_3Br$). Then, DE and CTAB-modified DE were converted to anatase phase TiO_2 replica microshells via a gas/solid displacement reaction followed by humid oxygen heat treatment using the method of Unocic *et al*.[55] The intention was to examine the advantages of conversion of TiO_2 replica microshells to $BaTiO_3$ utilizing a microwave assisted hydrothermal method over the conventional hydrothermal method.

3.2 Experimental Setup

3.2.1 CTAB Treatment of Diatomaceous Earth

DE was pretreated in order to increase the surface area. The surface treatment solution was prepared by introducing 3.05 g of CTAB into a 0.7M solution of NaOH (sodium hydroxide, Alfa Aesar) and stirring for 20 min. Next, 5.00 g of DE was added to the solution and stirred for 20 min. The suspension is sealed in a stainless steel vessel (2.4 cm I.D. × 15.2 cm L) and heat treated in an oven at 130 ºC for duration of 72 h. After the heat treatment, the treated frustules were filtered, heat treated to 540 ºC at 1 ºC/min and held for 1 h. The CTAB-treated DE was then stored in an argon controlled environment. Figure 3.1 shows a scanning electron microscopy (SEM) image of a DE frustule after CTAB treatment, in which, the macropores (> 50 nm) and channels are clearly visible. The treatment mainly affects the pores in the micropore range (<2 nm) and the mesopore range (2 nm – 50 nm) and, therefore, cannot be resolved in SEM.

Using the method of Brunauer-Emmett-Teller (BET),[60] Nitrogen (N_2) adsorption analysis (Autosorb-1C, Quantachrome, Boyton, FL) indicated an increase in the SSA of the DE from 1.6 m^2/g for DE to 197 m^2/g for the CTAB-treated DE.

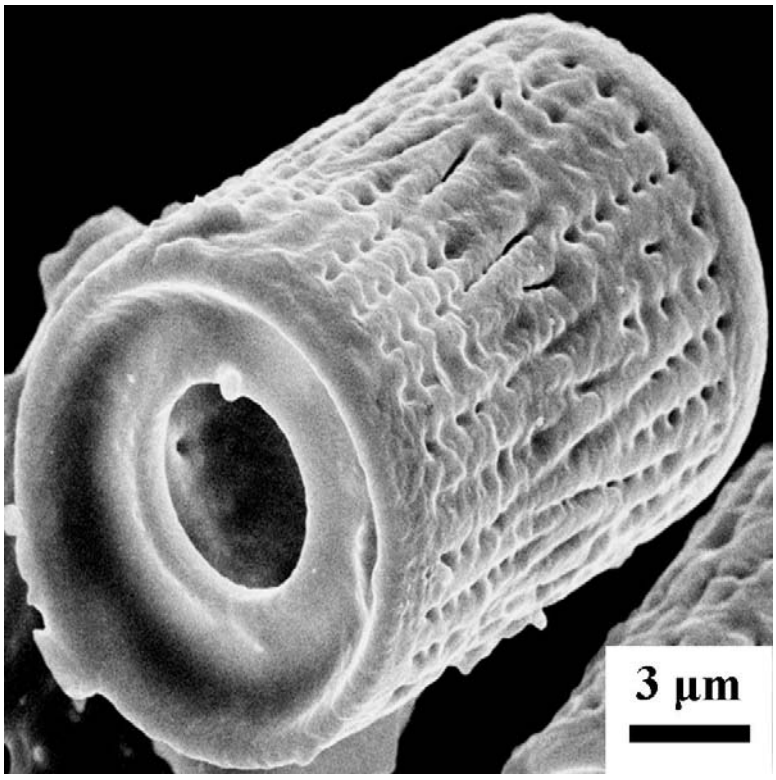

Figure 3.1 Secondary electron image of a diatomaceous earth frustule after CTAB treatment.

3.2.2 Conversion of SiO_2 Frustules into TiO_2 Replicas

The DE frustules (both CTAB-treated and non-CTAB-treated) were then converted to anatase phase TiO_2 via the method of Unocic et al.[55] 200 mg of DE-based frustules were placed in a homemade nickel (Ni) tray and sealed by welding in a titanium tube (2.54 cm I.D. × 16.99 cm L, titanium tubing, Grade 2, McMaster-Carr, Atlanta, GA)

containing 1.00 g of TiF_4 (titanium(IV) fluoride, Advanced Chemicals Research, Catoosa, OK). The tube was heat treated to 350 ºC at 5 ºC/min and maintained for 2 h, producing titanium oxide fluoride ($TiOF_2$). After removing the Ni tray from the tube, the $TiOF_2$ frustules were reheat treated in a magnesium oxide (MgO, Ozark Technical Ceramics, Webb City, MO) crucible to 400 ºC at 5 ºC/min and maintained for 5 h in an environment with oxygen flowing at 1 L/min through 70 ºC DI water to convert the $TiOF_2$ microshell replicas to TiO_2 microshells. After conversion, the DE replicas are seen to have maintained most of the nano- and microscale fine features (Figure 3.2). XRD analysis indicates complete conversion of the SiO_2 to TiO_2 (Figure 3.3).

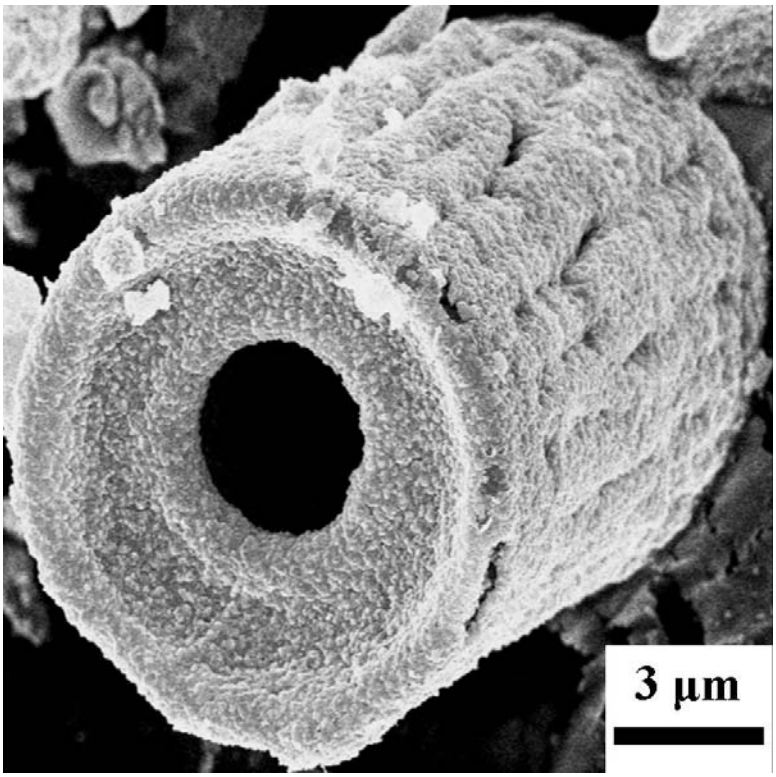

Figure 3.2 Secondary electron image of a diatomaceous earth frustule after CTAB treatment and conversion to TiO_2

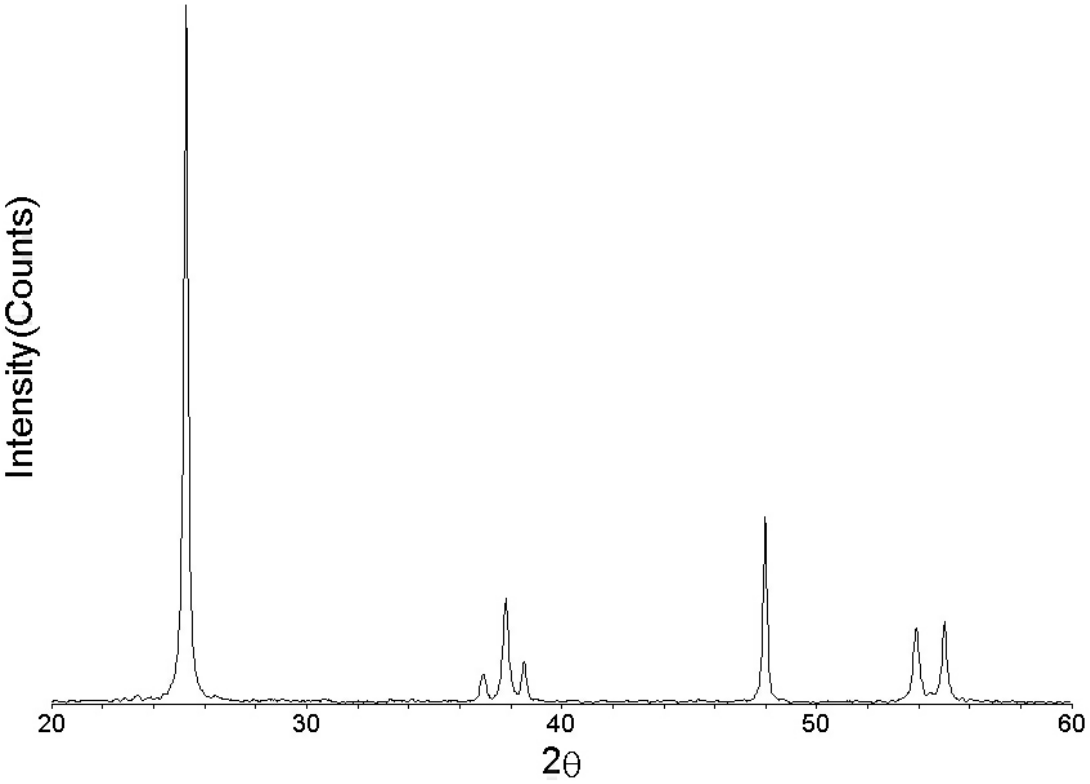

Figure 3.3 XRD pattern illustrating the complete conversion of CTAB treated SiO_2 frustules to TiO_2 replicas.

3.2.3 Hydrothermal Conversions of Microshells from TiO_2 into $BaTiO_3$

The microwave vessel employed for the $BaTiO_3$ conversion was a commercially prepared, CEM (XP-1500 Plus, CEM), MARS-5 vessel (3.3 cm I.D. × 11.8 cm L). The temperature of the vessel used in the microwave was measured via a microwave transparent fiber-optic temperature probe (RTP-300 Plus, CEM) protected by a sapphire tube which extends to the bottom of the inner liner of the vessel. Pressure was measured using an internal electronics sensor (ESP-1500, CEM). In order to make an equal comparison, the same type of vessel was used for both the microwave and conventional hydrothermal experiments.

$BaTiO_3$ replicas were prepared using TiO_2 microshells derived from both CTAB-modified and non-CTAB-modified frustules. 50 mg of TiO_2 microshells were introduced with 10 mL of boiled, DI (deionized) water into a vessel for each method and each type of microshell. In an argon controlled glove box, 5.0 g of barium hydroxide octahydrate ($Ba(OH)_2 \cdot 8H_2O$ 98+ %, Alfa Aesar) was added to each vessel, stirred for 30 s, and sealed hand-tight. After removing the vessels from the glove box, they were tightened to 5 ft-lb of torque. Two vessels (CTAB modified and non-CTAB modified based) were transferred to a drying oven preheated to 100 ºC. Two vessels were transferred to the microwave. The microwave was programmed for 100% of 1600 W and ramped to a temperature of 100 ºC within 1 min. The durations ranged form 2 h to 24 h for both methods. After the respective treatments, the specimens were washed six times using DI water. The specimens were washed in 500mM prepared acetic acid for 30 min, to dissolve barium carbonate formed on the surface due to exposure to air after hydrothermal treatment. Following the acid treatment, the specimens were washed 5 times using DI water and dried at 90 ºC for 24 h.

The particle size and morphology of the converted microshells was investigated by SEM (LEO-1530, Zeiss, Germany). The composition of the microshells was studied with X-ray diffraction (Alpha-1, Panalytical, Netherlands) and electron dispersive spectroscopy (EDS). Scherrer analysis was used to calculate crystallite size information from full-width-at-half-maximum (FWHM) in XRD peak profiles. The pore structure of the frustules was studied using N_2 gas adsorption. TGA (thermogravimetric analysis, STA 449C, Netzsch, Burlington, MA) was performed to measure weight loss.

3.3 Results and Discussion

X-ray diffraction analysis was performed on all of the specimens, between 20º to 60º 2θ. A silicon powder standard was used to establish peak positions. The peaks shifted by less than 0.006º 2θ, and the full width at half maximum (FWHM) was less than 0.078º 2θ. All of the specimens exhibited peaks corresponding to the cubic phase of $BaTiO_3$ (PDF 31-0174), the anatase phase of TiO_2 (PDF 21-1272), or both.

In order to estimate the amount of conversion with time, standards were made with $BaTiO_3$ powder (Sigma Aldrich) and anatase TiO_2 powder (Alfa Aesar). The standards were mixed in 10 weight percent (wt. %) increments from 10 wt. % $BaTiO_3$ and 90 wt. % TiO_2 to 90 wt. % $BaTiO_3$ and 10 wt % TiO_2. Additional compositions were made for 95, 97, 98, and 99 wt. % $BaTiO_3$. The ratio of the area for the (110) peak of $BaTiO_3$ to the area for the (101) peak of TiO_2 were calculated for each specimen by fitting the peak profiles (*Jade 7, XRD Pattern Processing, Identification and Quantification*). These ratios were plotted against the wt. % of $BaTiO_3$ (Figure 3.4)**.** A curve was fit to the plot in order to extract estimates for the amount of conversion based on the ratios of these peaks for each specimen.

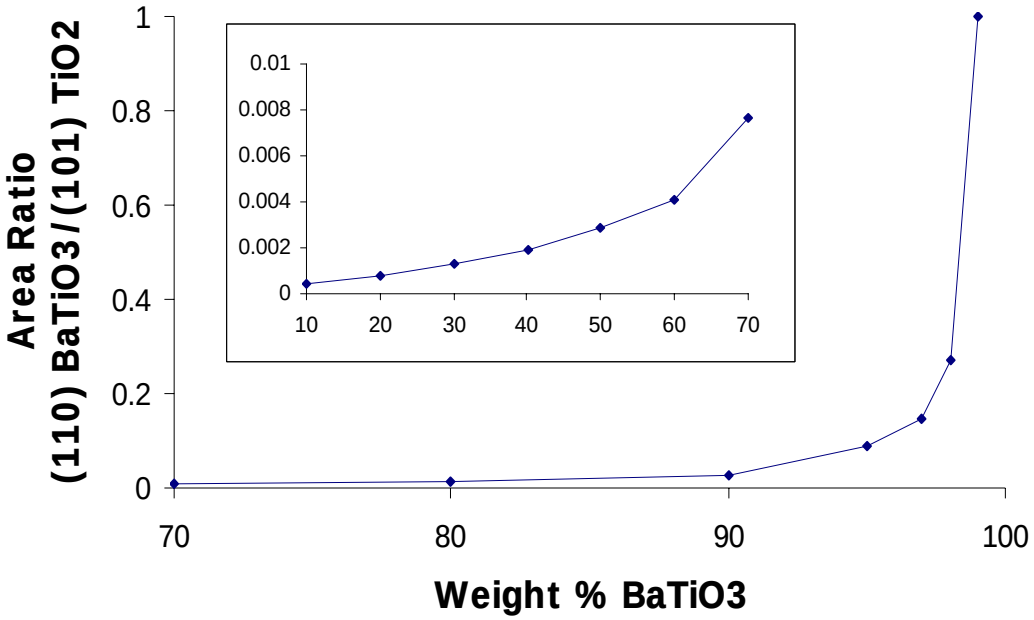

Figure 3.4 Plot illustrating the correlation between XRD peak area ratios for the main peaks of $BaTiO_3$ and TiO_2 to the known weight percents of $BaTiO_3$. The ratios have been normalized to the 99.0 weight percent $BaTiO_3$ ratio.

Figure 3.5 illustrates the wt. % of $BaTiO_3$ evolved from the TiO_2 specimens using the microwave and conventional hydrothermal methods between 30 min and 16 h of conversion. After 30 min, the microwave $BaTiO_3$ derived from CTAB-TiO_2 (CTAB-MBT) exhibited 52.9 wt. % of conversion in contrast to the $BaTiO_3$ from non-CTAB-TiO_2 (MBT) which exhibited only 3.6 wt. % of conversion. Neither the conventional $BaTiO_3$ derived from CTAB-TiO_2 (CTAB-BT) nor the non-CTAB TiO_2 (BT) exhibited measurable amounts of conversion. Both microwave assisted specimens exhibited greater amounts of conversion within the first 2 h, after which, the CTAB-MBT and the CTAB-BT experienced the greatest amounts of conversion. The majority of conversion for the highly reactive CTAB-TiO_2 specimens occurred within 8 h for both microwave

and conventional $BaTiO_3$. The MBT and BT specimens required 16 h to reach a maximum amount of conversion which failed to attain the wt. % of conversion found in the CTAB related specimens. The XRD patterns illustrate the increase in the extent of reaction after, 30 min, 2 h, 4 h, 8 h, and 16 h (Figure 3.6 - 3.10). Figure 3.11 illustrates the XRD patterns for the most converted CTAB-MBT and the least converted BT specimens.

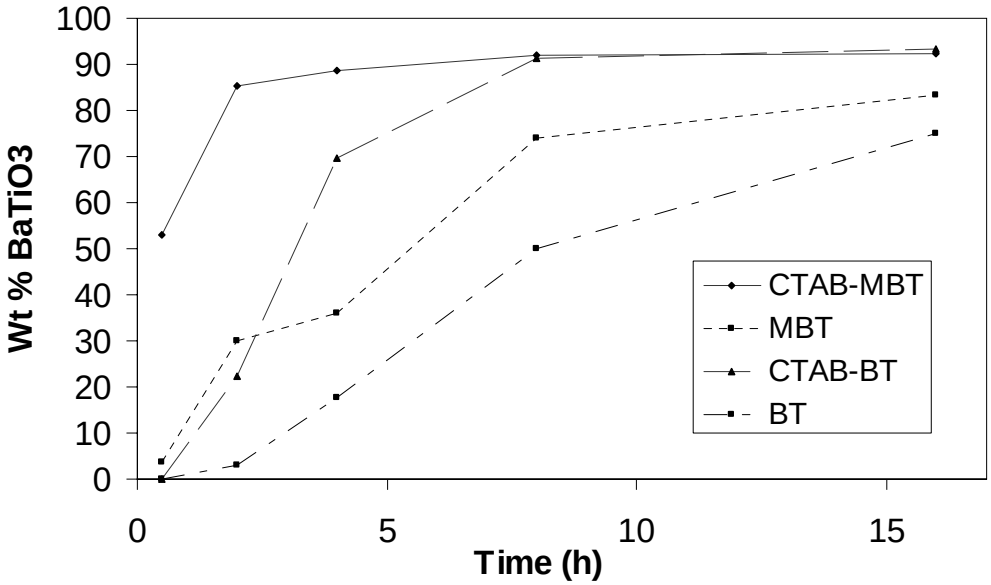

Figure 3.5 Plot of the wt. % $BaTiO_3$ for microwave and conventional hydrothermal specimens vs. time of conversion.

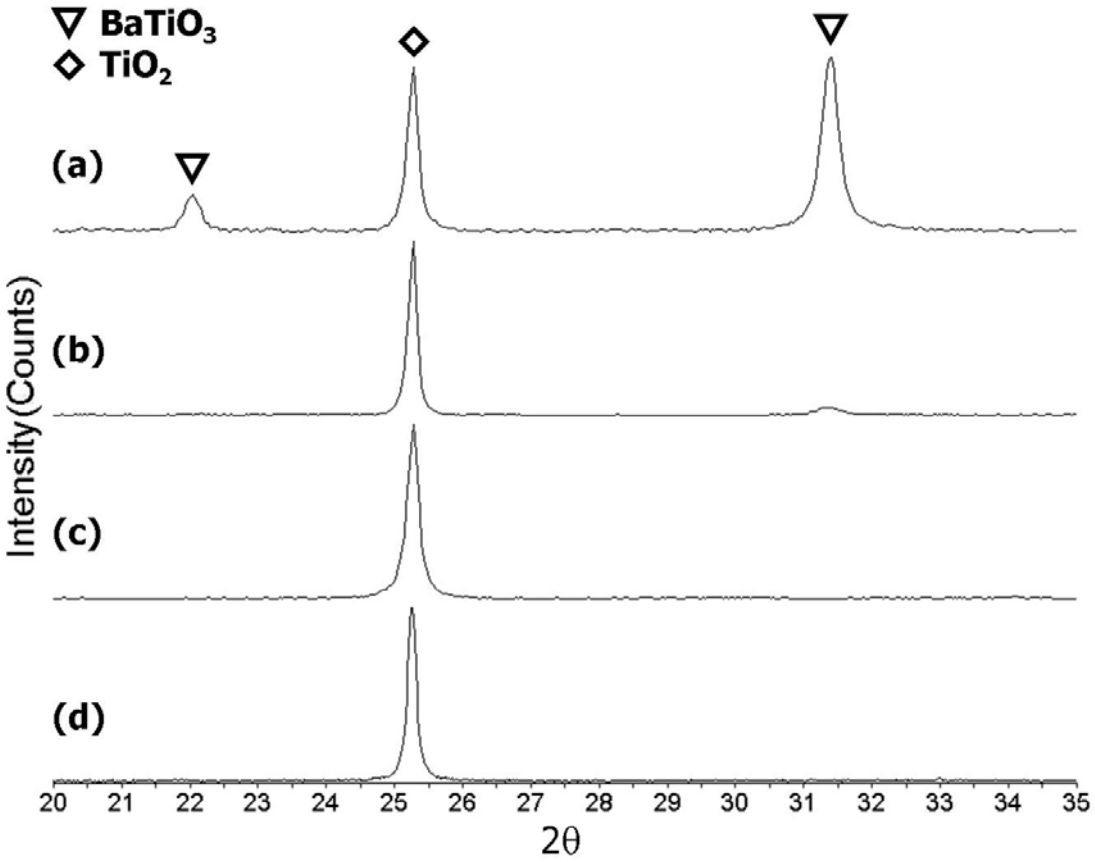

Figure 3.6 XRD patterns of the TiO_2 specimens after 30 min of conversion to: (a) CTAB-MBT, (b) MBT, (c) CTAB-BT, (d) BT.

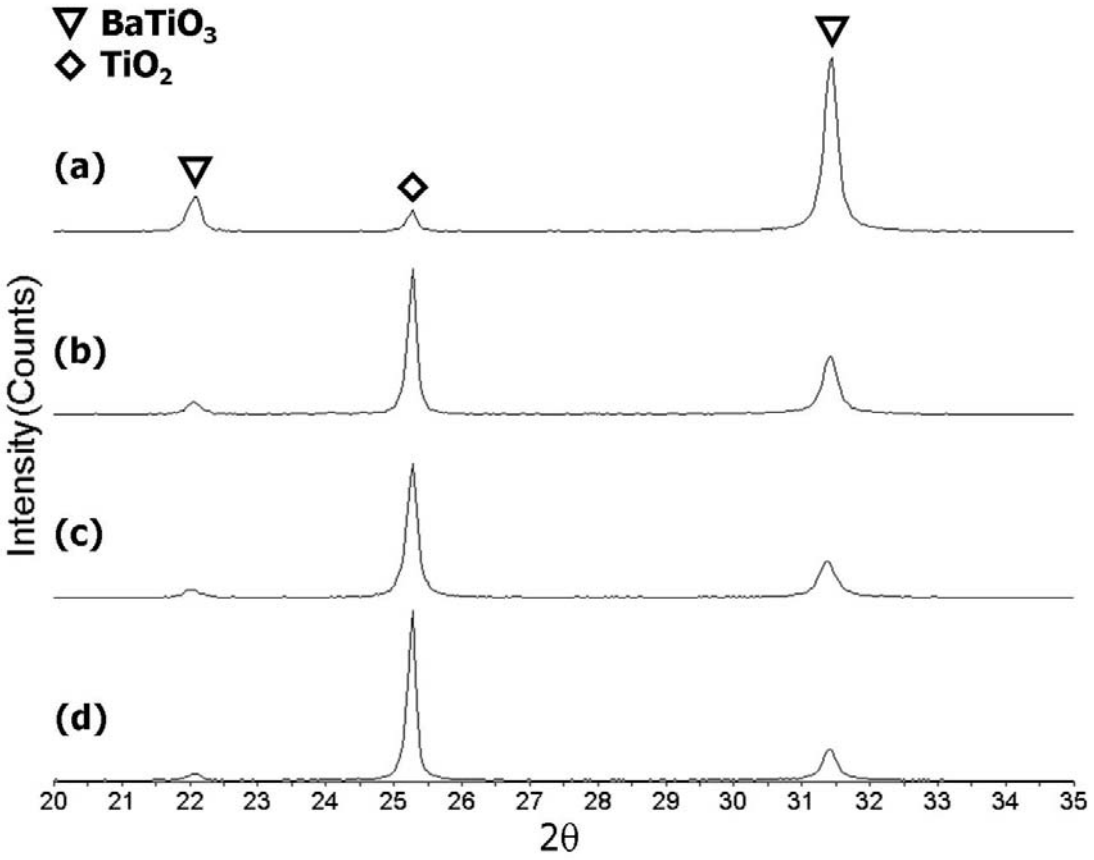

Figure 3.7 XRD patterns of the TiO_2 specimens after 2 h of conversion to: (a) CTAB-MBT, (b) MBT, (c) CTAB-BT, (d) BT.

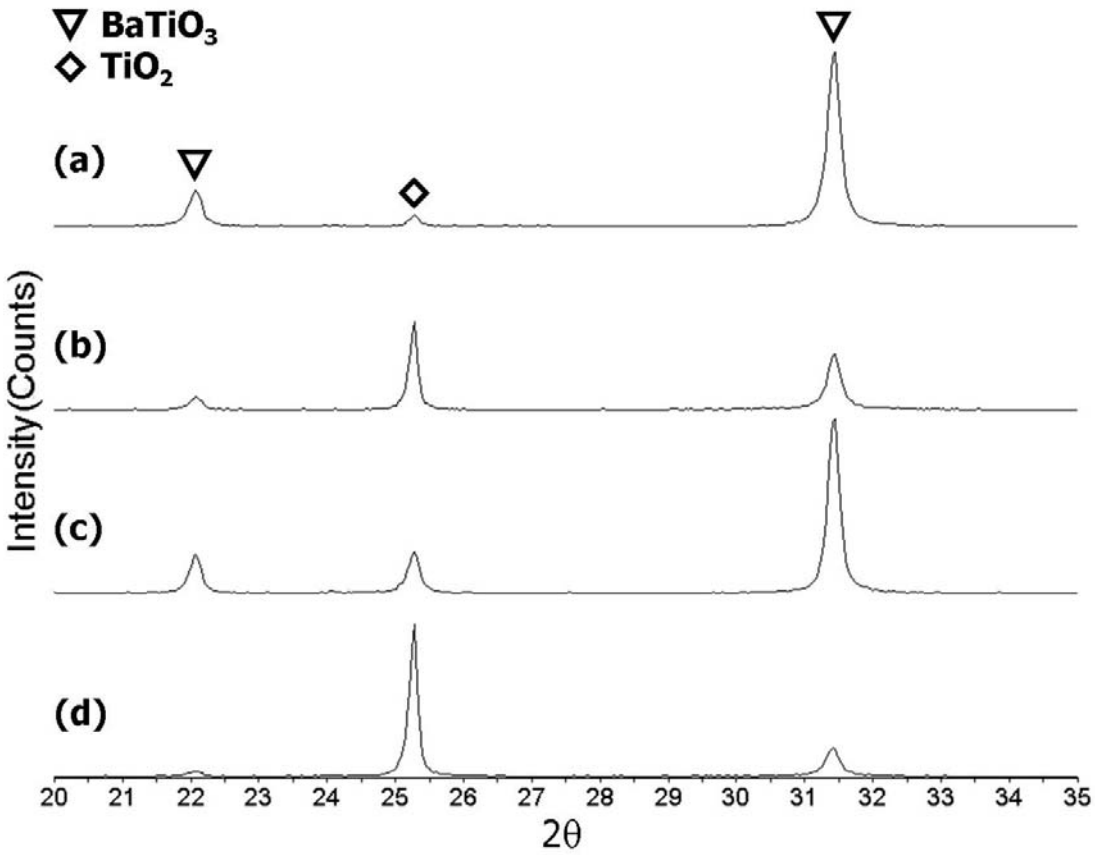

Figure 3.8 XRD patterns of the TiO_2 specimens after 4 h of conversion to: (a) CTAB-MBT, (b) MBT, (c) CTAB-BT, (d) BT.

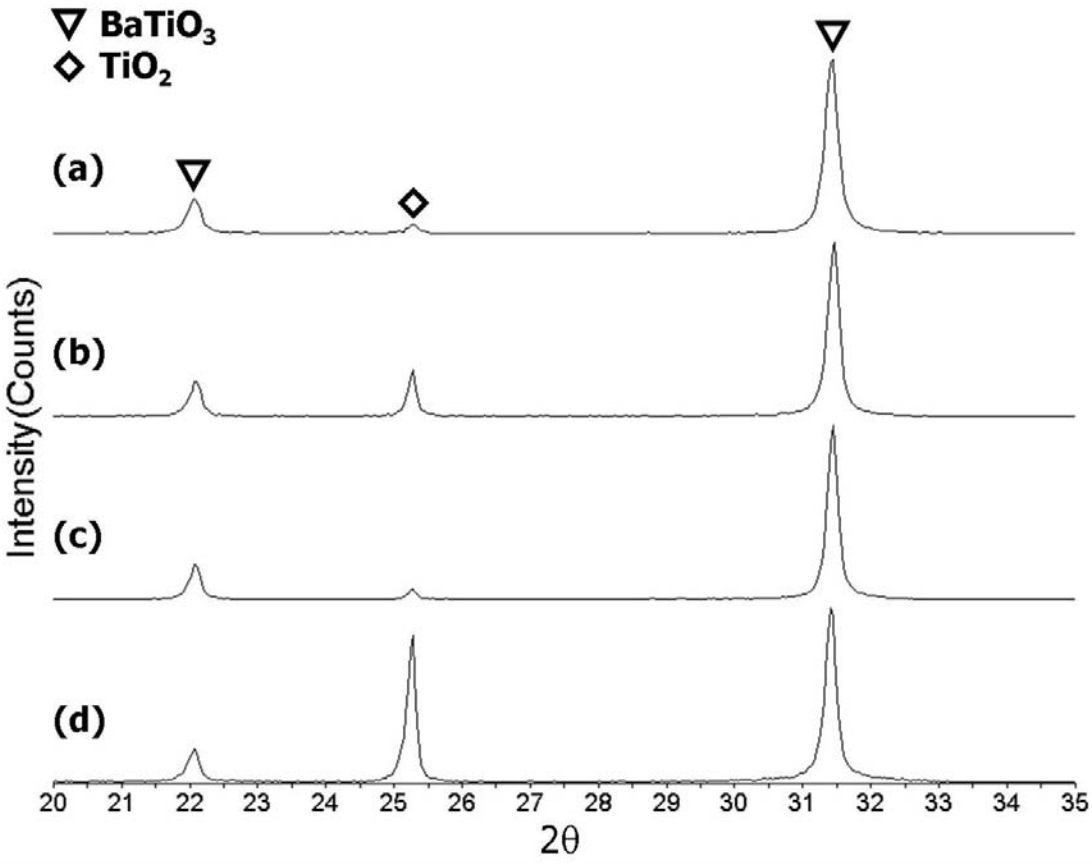

Figure 3.9 XRD patterns of the TiO_2 specimens after 8 h of conversion to: (a) CTAB-MBT, (b) MBT, (c) CTAB-BT, (d) BT.

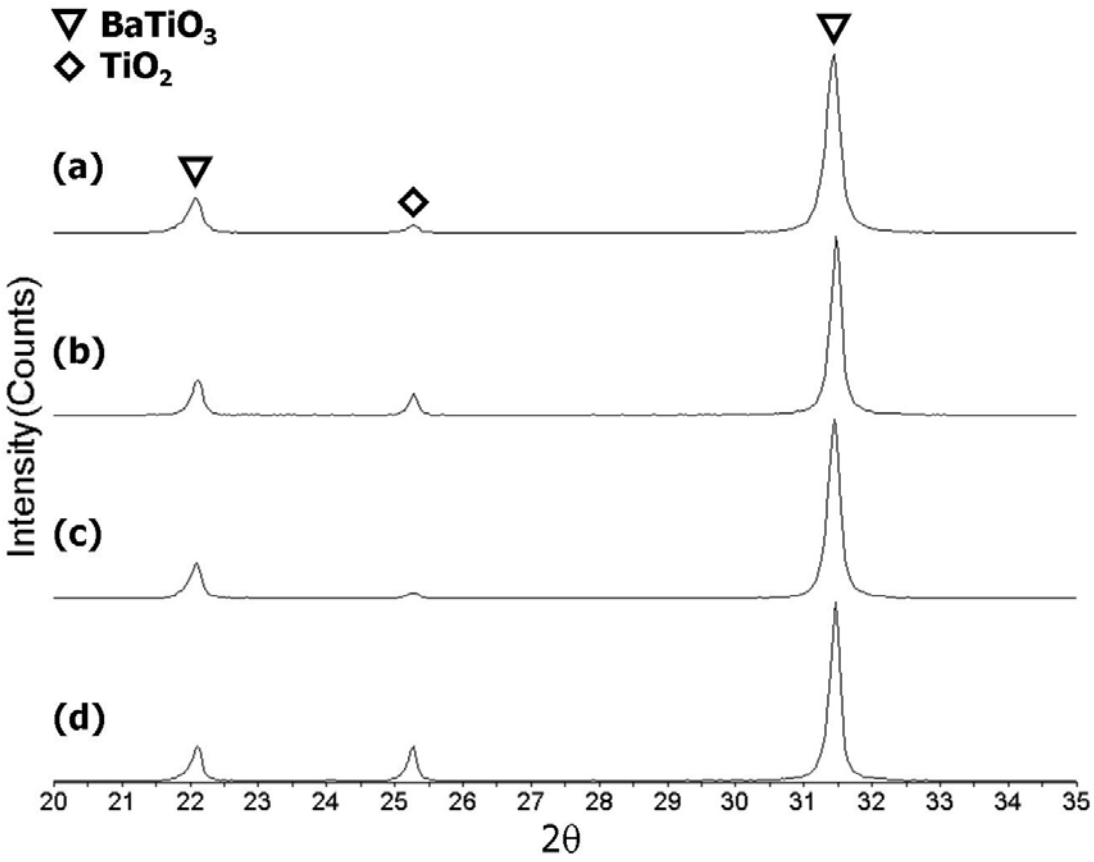

Figure 3.10 XRD patterns of the TiO_2 specimens after 16 h of conversion to: (a) CTAB-MBT, (b) MBT, (c) CTAB-BT, (d) BT.

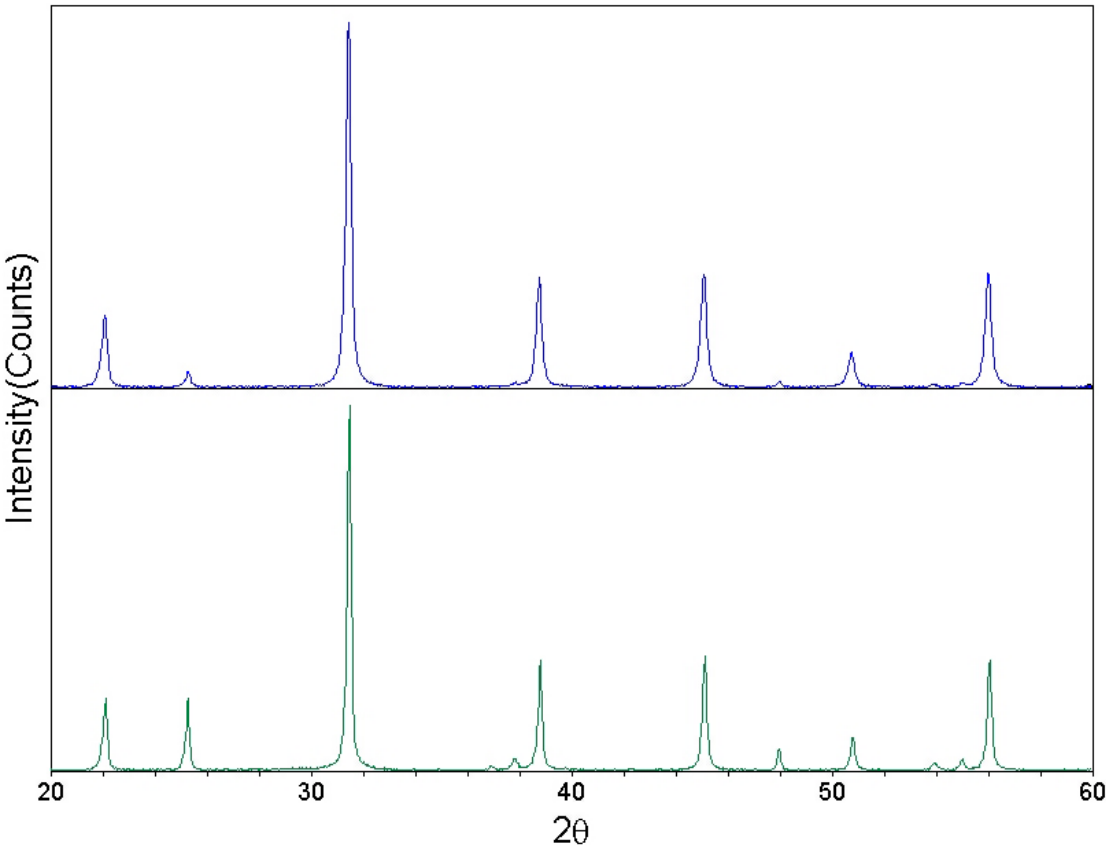

Figure 3.11 XRD patterns of CTAB-MBT and BT to illustrate the extremes in wt.% of $BaTiO_3$ after 16 h of conversion.

Scherrer analysis was used to calculate the average crystallite size for each specimen (Table 3.1). The average crystallite size was found to be 47 ± 2 nm, for the CTAB-MBT specimen after 16 h of conversion. Larger crystallite sizes were calculated for MBT specimens (81 ± 7 nm) compared to the CTAB-MBT specimens. Specimens which originated from CTAB-modified DE, possessed smaller crystallite sizes and lower dispersion compared to specimens originating from the untreated DE.

Table 3.1 Average crystallite sizes for all the specimens, after 16 h of conversion

Specimen	*Average Crystallite Size (nm)*
BT	85 ± 6
CTAB-BT	74 ± 3
MBT	98 ± 8
CTAB-MBT	54 ± 2

SEM was used to characterize the morphology of the frustules before and after conversion. Figure 3.12 (a and b) show images of a CTAB-MBT frustule and a CTAB-BT frustule, after 16 h of conversion. The images illustrate the preservation of the cylindrical shape. The morphologies are similar for all the specimens examined, therefore, it can be inferred that the reactions do not favor specific sites on the microshells and the rate of conversion is dependent on the diffusion through the walls of the microshells.

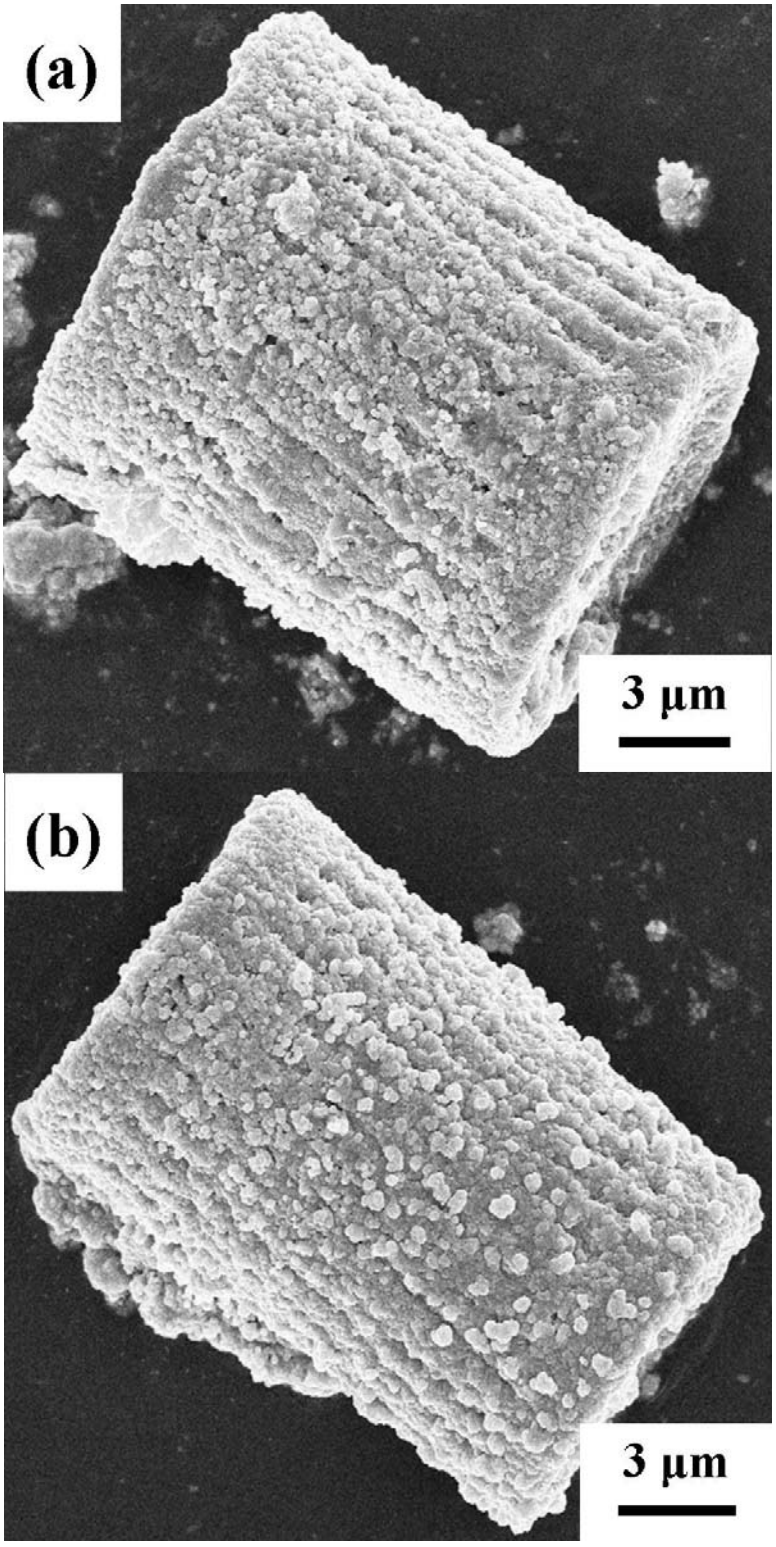

Figure 3.12 Secondary electron images of CTAB-TiO_2 frustules after 16 h of conversion to $BaTiO_3$ via: (a) microwave and (b) conventional heating methods.

The average particle sizes of the CTAB-MBT and CTAB-BT specimens after 16 h of conversion were measured to be 151 ± 40 nm and 177 ± 60 nm, respectively. This observation for particle size is in agreement with the observations of Jhung *et al*., who attributed the larger particle size of $BaTiO_3$ derived from conventional hydrothermal to the slow nucleation kinetics.[61] In contrast, Sun *et al*. observed larger particle sizes and larger dispersion during microwave assisted hydrothermal synthesis which yielded the tetragonal phase of $BaTiO_3$.[50] The larger particle size would be desirable given the findings of Uchino *et al*.[62] and Begg *et al*.[63] who discovered $BaTiO_3$ may require a minimum particle size in order to allow for the cubic to tetragonal transformation upon cooling to room temperature.[62-65]

Gas adsorption was performed using N_2 at liquid nitrogen temperature (195.9 ºC). The method of Barrett-Joyner-Halenda was used to interpret the adsorption and desorption isotherms to calculate pore size distribution.[66] Neither micropores nor mesopores were present in appreciable amounts between 0.3 atm and 1 atm. Therefore, the majority of the pores must lie in a macropore range out of the detectable range by our instrument. In order to accurately measure macropores of this size, other methods such as mercury porosimetry must be used. BET analysis of the CTAB-MBT and CTAB-BT, after 8 h of conversion, yielded specific surface areas of 11.6 m^2/g and 4.4 m^2/g, respectively. These values are similar to the specific surface areas from the starting anatase specimens which yielded 11.3 m^2/g for the CTAB-treated and 4.9 m^2/g for the regular TiO_2 replicas, implying negligible changes in the specific surface areas.

Weight loss of the CTAB-MBT and CTAB-BT converted for 16 h was measured for a duration of 12 h at 1150 ºC. In parallel, this was an attempt to heat-treat the cubic

phase of $BaTiO_3$ for an extended duration in order to transform to the tetragonal phase upon cooling to room temperature. Based on a study by Clark *et al*., the ratio of the *c* and *a* lattice constants for cubic/tetragonal $BaTiO_3$ begins to asymptotically approach the maximum at 1150 ºC, which corresponds to a *c/a* greater than 1.008.[67]

The total weight loss experienced by the CTAB-MBT and the CTAB-BT specimens over the entire heat treatment was 2.8 and 2.5 %, respectively. Figure 3.13 shows plots of weight loss during the initial ramp from room temperature to 1150 ºC for both specimens. During the first stage of weight loss between room temperature and 175 ºC, CTAB-MBT specimen experienced a weight loss of 0.8 % while the CTAB-BT only experienced a 0.6 % loss. Each loss is associated with desorption of physisorbed water on the surface and between the macroporous structure of the converted frustules.[39, 68, 69] Second and third segments are subject to interpretation. Between 175 and 800 °C, the specimens experienced weight losses of approximately 1.6 % for both specimens which is attributed to diffusion of OH^- ions to the grain boundaries followed by evaporation from the specimen, which has been reported to terminate at lower temperatures.[63, 68-71] Potdar *et al*. attributed weight loss at temperatures above 500 °C to decomposition reactions of the form:

$$BaCO_3\ (s) + TiO_2\ (s) \rightarrow BaTiO_3\ (s) + CO_2\ (g)$$

followed by the diffusion of CO_2 to surfaces where it evaporates.[39] Similar observations were made by Newalker *et al*. who found the carbonate decomposition threshold to lie above 800 °C.[68, 70, 71] The final weight loss in both specimens was approximately 0.2 %.

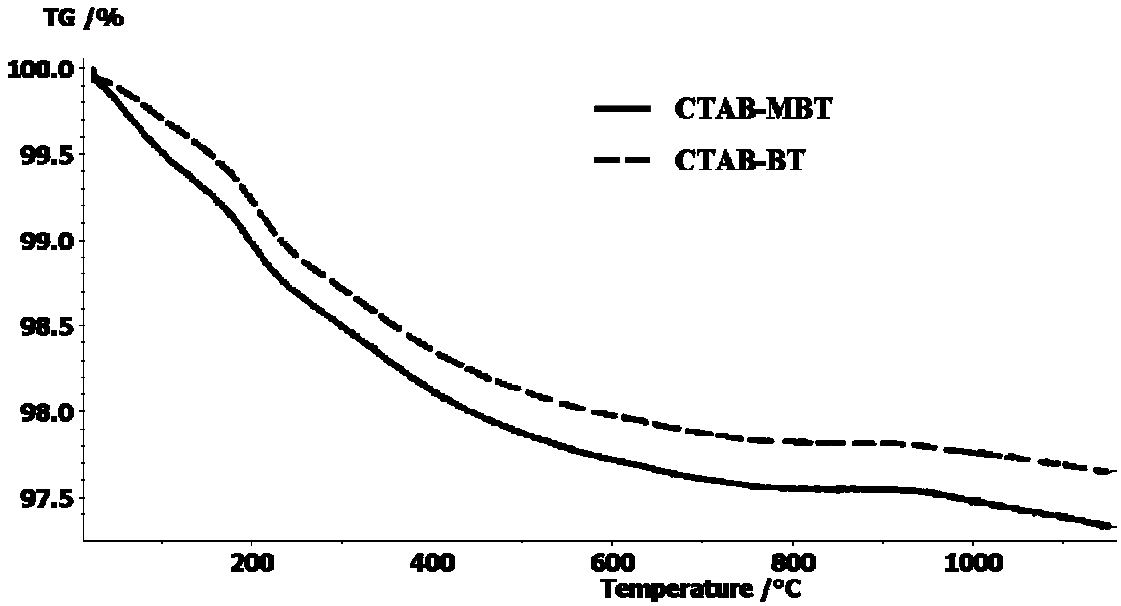

Figure 3.13 Thermogravimetric analysis results for CTAB-MBT and CTAB-BT after 16 h of conversion.

XRD analysis, performed after heat-treatment, yielded multiple barium titanium oxide phases, but not the tetragonal phase which was expected (Figure 3.14). The cubic phase of $BaTiO_3$ appears present, but peak shifted either from lattice strain due to the presence of other phases. Among the other phases yielded during the heat-treatment, $Ba_4Ti_{13}O_{30}$ was a minority phase. O'Bryan and Thomson found the formation of this phase to occur in the TiO_2-rich region of the BaO-TiO_2 system.[72] Formation of this phase could be attributed to the presence of unreacted TiO_2. Hertl determined that the diffusion of Ba^{2+} through $BaTiO_3$ is negligible compared with the reaction time required to react with TiO_2.[45] Therefore, $Ba_4Ti_{13}O_{30}$ might have formed at a $BaTiO_3$-TiO_2 boundary. When combined with elevated temperatures for an extended period of time, Ba^{2+} ions

would possess the driving force to diffuse from the Ba-rich region ($BaTiO_3$) to the Ba-lean region (TiO_2) producing $Ba_4Ti_{13}O_{30}$.

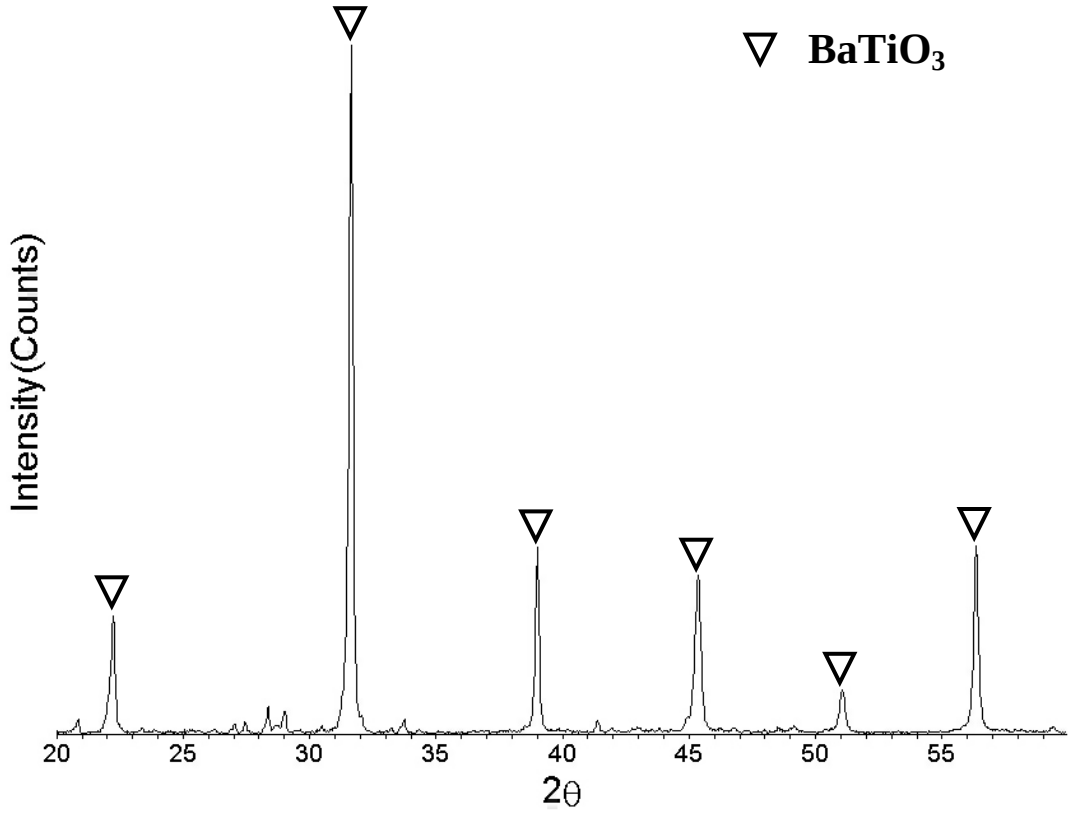

Figure 3.14 XRD pattern of the CTAB-MBT specimen after 16 h of conversion, followed by 12 h of heat treatment in the TGA at 1150 ºC.

3.4 Conclusion

Microwave and conventional hydrothermal conversion methods were compared to determine the advantage of using microwave heating to assist in the conversion of SiO_2 DE frustules to $BaTiO_3$ replicas. The microwave assisted reactions occurred faster than the conventional conversions during the beginning of the conversion period for both the

CTAB-treatment based and non-CTAB-treatment based specimens. In both hydrothermal methods, the CTAB-treatment-based specimens were observed to experience greater extents of conversion and require less time to attain their conversion maxima. All the specimens exhibited similar morphological structures and particle sizes. The desired tetragonal phase of $BaTiO_3$ was not obtained after hydrothermal treatment or after post-hydrothermal heat-treatment to 1150 ºC. Microwave assisted hydrothermal conversion does accelerate the initial period of the conversion, but was not observed to drive the conversion to completion faster than the conventional hydrothermal method.

3.5 References

1. C. J. Johnson: Some dielectric and electro-optic properties of BaTiO3 single crystals. *Applied Physics Letters*. **7,** 221 (1965).

2. T. C. Rutt and J. A. Stynes: Fabrication of multilayer ceramic capacitors by metal impregnation. *IEEE Transactions on Parts, Hybrids, and Packaging*. **9,** 144 (1973).

3. H. Igarashi, C. Betoh and K. Okazaki: Vapor-phase diffusion of metal oxides into barium titanate(IV) ceramics and its application to multilayer boundary layer capacitors. *Advances in Ceramics*. **1,** 254 (1981).

4. R. Wernicke: Ceramic multilayer capacitors and nonlinear resistors. *Science of Ceramics*. **12,** 677 (1984).

5. H. J. Hagemann, D. Hennings and R. Wernicke: Ceramic multilayer capacitors. *Philips Technical Review*. **41,** 89 (1984).

6. P. D. Levett: Properties and applications of positive temperature coefficients thermistors. *Ceramic Age*. **83,** 44 (1967).

7. J. Daniels, K. H. Haerdtl and R. Wernicke: The PTC effect of barium titanate. *Philips Technical Review*. **38,** 73 (1979).

8. M. Kuwabara: Explanation for the PTCR effect in barium titanate ceramics. *Advances in Ceramics*. **7,** 128 (1983).

9. G. V. Lewis, C. R. A. Catlow and R. E. W. Casselton: PTCR effect in barium titanate (BaTiO3). *Journal of the American Ceramic Society*. **68,** 555 (1985).

10. B. M. Kulwicki: Trends in PTC resistor technology. *Electron. Mater. Processes, Int. SAMPE Electron. Conf., 1st*. 441 (1987).

11. R. Ford and M. Kahn: Positive temperature coefficient resistors as high-power pulse switches: performance limitations, temperature effects, and triggering behavior. *Journal of Applied Physics*. **61,** 2381 (1987).

12. L. S. Lukic, Z. Preradovic, V. Dimic, D. Stefanovic and L. Vulicevic: Prognosis the properties of BaTiO3 ceramics for piezoelectric transducers. *Sintering and Materials, Proceedings of the International Symposium on the Science and Technology of Sintering, 6th, Haikou, Peop. Rep. China, Oct. 23-25, 1995*. 250 (1995).

13. D. Stefanovic, V. Dimic, M. Radmanovic, D. Mancic, L. Lukic and L. Vulicevic: Synthesis of BaTiO3 ceramics for piezoelectric transducers. *Science of Sintering*. **28,** 51 (1996).

14. G. H. Haertling: Ferroelectric ceramics: history and technology. *Journal of the American Ceramic Society*. **82,** 797 (1999).

15. K. Kiss, J. Magder, M. S. Vukasovich and R. J. Lockhart: Ferroelectrics of ultrafine particle size. I. Synthesis of titanate powders of ultrafine particle size. *Journal of the American Ceramic Society*. **49,** 291 (1966).

16. K. S. Mazdiyasni, R. T. Dolloff and J. S. Smith, II: Preparation of high-purity submicron barium titanate powders. *Journal of the American Ceramic Society*. **52,** 523 (1969).

17. D. Chen and X. Jiao: Solvothermal synthesis and characterization of barium titanate powders. *Journal of the American Ceramic Society*. **83,** 2637 (2000).

18. H. I. Won, H. H. Nersisyan and C. W. Won: Low temperature solid-phase synthesis of tetragonal BaTiO3 powders and its characterization. *Materials Letters*. **61,** 1492 (2007).

19. A. E. Feuersanger, A. K. Hagenlocher and A. L. Solomon: Preparation and properties of thin barium titanate films. *Journal of the Electrochemical Society*. **111,** 1387 (1964).

20. C. H. Lee and S. J. Park: Preparation of ferroelectric barium titanate thin films by metal organic chemical vapor deposition. *Journal of Materials Science: Materials in Electronics*. **1,** 219 (1990).

21. M. Yoshimura, S. E. Yoo, M. Hayashi and N. Ishizawa: In situ preparation of barium titanate (BaTiO3) thin film by hydrothermal-electrochemical synthesis. *Ceramic Transactions*. **15,** 427 (1990).

22. K.-M. Hung, C.-S. Hsieh, W.-D. Yang and Y.-J. Sun: The preparatory optimal conditions of barium titanate thin film from a hydrothermal method at low temperature. *Journal of Materials Science*. **42,** 2376 (2007).

23. J. F. Scott: Dimensional effects on ferroelectrics. Ultra-thin single crystals, nanotubes, nano-rods, and nano-ribbons. *Ferroelectrics*. **316,** 13 (2005).

24. S. J. Limmer, S. Seraji, Y. Wu, T. P. Chou, C. Nguyen and G. Cao: Template-based growth of various oxide nanorods by sol-gel electrophoresis. *Advanced Functional Materials*. **12,** 59 (2002).

25. J. H. Wei, J. Shi, Z. Y. Liu and J. B. Wang: Polymer-assisted synthesis of BaTiO3 nanorods. *Journal of Materials Science*. **41,** 3127 (2006).

26. J. Y. Choi, C. H. Kim and D. K. Kim: Hydrothermal synthesis of spherical perovskite oxide powders using spherical gel powders. *Journal of the American Ceramic Society*. **81,** 1353 (1998).

27. T. Yan, X.-L. Liu, N.-R. Wang and J.-F. Chen: Synthesis of monodispersed barium titanate nanocrytals - hydrothermal recrystallization of BaTiO3 nanospheres. *Journal of Crystal Growth*. **281,** 669 (2005).

28. X. Zhu, J. Zhu, S. Zhou, Z. Liu, N. Ming and D. Hesse: BaTiO3 nanocrystals: hydrothermal synthesis and structural characterization. *Journal of Crystal Growth*. **283,** 553 (2005).

29. S. Yoon, S. Baik, M. G. Kim, N. Shin and I. Kim: Synthesis of tetragonal barium titanate nanoparticles via alkoxide-hydroxide sol-precipitation: effect of water addition. *Journal of the American Ceramic Society*. **90,** 311 (2007).

30. B. A. Hernandez, K.-S. Chang, E. R. Fisher and P. K. Dorhout: Sol-gel template synthesis and characterization of BaTiO3 and PbTiO3 nanotubes. *Chemistry of Materials*. **14,** 480 (2002).

31. N. P. Padture and X. Wei: Hydrothermal synthesis of thin films of barium titanate ceramic nano-tubes at 200 DegC. *Journal of the American Ceramic Society*. **86,** 2215 (2003).

32. Y. Luo, I. Szafraniak, N. D. Zakharov, V. Nagarajan, M. Steinhart, R. B. Wehrspohn, J. H. Wendorff, R. Ramesh and M. Alexe: Nanoshell tubes of ferroelectric lead zirconate titanate and barium titanate. *Applied Physics Letters*. **83,** 440 (2003).

33. J. E. Spanier, J. J. Urban, L. Ouyang, W. S. Yun and H. Park: Ferroelectric nanowires. *Nanowires and Nanobelts*. **2,** 83 (2003).

34. J. J. Urban, J. E. Spanier, L. Ouyang, W. S. Yun and H. Park: Single-crystalline barium titanate nanowires. *Advanced Materials (Weinheim, Germany)*. **15,** 423 (2003).

35. U. A. Joshi, S. Yoon, S. Baik and J. S. Lee: Surfactant-Free Hydrothermal Synthesis of Highly Tetragonal Barium Titanate Nanowires: A Structural Investigation. *Journal of Physical Chemistry B*. **110,** 12249 (2006).

36. D. E. Rase and R. Roy: Phase Equilibria in the System BaO-TiO_2. *Journal of the American Ceramic Society*. **38,** 102 (1955).

37. D. F. K. Hennings, B. S. Schreinemacher and H. Schreinemacher: Solid State Preparation of $BaTiO_3$-Based Dielectrics, Using Ultrafine Raw Materials. *Journal of the American Ceramic Society*. **84,** 2777 (2001).

38. D. Hennings and W. Mayr: Thermal Decomposition of (BaTi) Citrates into Barium Titanate. *Journal of Solid State Chemistry*. **26,** 329 (1978).

39. H. S. Potdar, S. B. Deshpande and S. K. Date: Chemical coprecipitation of mixed (Ba + Ti) oxalates presursor leading to $BaTiO_3$ Powders. *Materials Chemistry and Physics*. **58,** 121 (1999).

40. M. Stockenhuber, H. Mayer and J. A. Lercher: Preparation barium titanate from oxalates. *Journal of the American Ceramic Society*. **76,** 1185 (1993).

41. P. Pinceloup, C. Courtois, A. Leriche and B. Thierry: Hydrothermal Synthesis of Nanometer-Sized Barium Titanate Powders: Control of Barium/Titanium Ratio, Sintering, and Dielectric Properties. *Journal of the American Ceramic Society*. **82,** 3049 (1999).

42. X. Wang, B. I. Lee, M. Z. Hu, E. A. Payzant and D. A. Blom: Mechanism of nanocrystalline $BaTiO_3$ particle formation by hydrothermal refluxing synthesis. *Journal of Materials Science: Materials in Electronics*. **14,** 495 (2003).

43. B. W. Lee and G. S. Choi: Hydrothermal synthesis of barium titanate powders from a co-precipitated precursor. *Journal of Ceramic Processing Research*. **4,** 151 (2003).

44. M. Boulos, S. Guillemet-Fritsch, F. Mathieu, B. Durand, T. Lebey and V. Bley: Hydrothermal synthesis of $BaTiO_3$ powders and dielectric properties of corresponding ceramics. *Solid State Ionics*. **176,** 1301 (2005).

45. W. Hertl: Kinetics of Barium Titanate Synthesis. *Journal of the American Ceramic Society*. **71,** 879 (1988).

46. G. Pfaff: $BaTiO_3$ Preparation by Reaction of TiO_2 with $Ba(OH)_2$. *Journal of the European Ceramic Society*. **8,** 35 (1991).

47. J. O. Eckert, Jr., C. C. Hung-Houston, B. L. Gersten, M. M. Lencka and R. E. Riman: Kinetics and Mechanics of Hydrothermal Synthesis of Barium Titanate. *Journal of the American Ceramic Society*. **79,** 2929 (1996).

48. M. Wu, J. Long, G. Wang, A. Huang and Y. Luo: Hydrothermal Synthesis of Tetragonal Barium Titanate from Barium Hydroxide and Titanium Dioxide under Moderate Conditions. *Journal of the American Ceramic Society*. **82,** 3254 (1999).

49. S. Komarneni, R. Roy and Q. H. Li: Microwave-hydrothermal synthesis of ceramic powders. *Materials Research Bulletin*. **27,** 1393 (1992).

50. W. Sun, J. Li, W. Liu and C. Li: Preparation of fine tetragonal barium titanate powder by a microwave-hydrothermal process. *Journal of the American Ceramic Society*. **89,** 118 (2006).

51. L. Guo, H. Luo, J. Gao, L. Guo and J. Yang: Microwave hydrothermal synthesis of barium titanate powders. *Materials Letters*. **60,** 3011 (2006).

52. K. H. Sandhage: Shape microcomponents via reactive conversion of biologically-derived microtemplates. *U.S. Patent No. 7,067,104*, June 27, 2006.

53. K. H. Sandhage, M. B. Dickerson, P. M. Huseman, M. A. Caranna, J. D. Clifton, T. A. Bull, T. J. Heibel, W. T. Overton and M. E. A. Schoenwaelder: Novel, bioclastic route to self-assembled, 3-D, chemically tailored meso/nanostructures: Shape-preserving reactive conversion of biosilica (diatom) microshells. *Advanced Materials*. **14,** 429 (2002).

54. F. M. Zalar, M. B. Dickerson and K. H. Sandhage: *Self-Assembled, 3-D Nanoparticle Structures with Tailored Chemistries via the BaSIC Process*, (ASM International, Materials Park, OH, 2003).

55. R. R. Unocic, F. M. Zalar, P. M. Sarosi, Y. Cai and K. H. Sandhage: Anatase assemblies from algae: Coupling biological self-assembly of 3-D nanoparticle structures with synthetic reaction chemistry. *Chemical Communications*. **7,** 795 (2004).

56. Y. Cai, S. M. Allan, F. M. Zalar and K. H. Sandhage: Three-dimensional magnesia-based nanocrystal assemblies via low-temperature magnesiothermic reaction of diatom microshells. *Journal of the American Ceramic Society*. **88,** 2005 (2005).

57. S. Shian, Y. Cai, M. R. Weatherspoon, S. M. Allan and K. H. Sandhage: Three-dimensional assemblies of zirconia nanocrystals via shape-preserving reactive conversion of diatom microshells. *Journal of the American Ceramic Society*. **89,** 694 (2006).

58. E. M. Ernst, B. C. Church, C. S. Gaddis, R. L. Snyder and K. H. Sandhage: Enhanced hydrothermal conversion of surfactant-modified diatom microshells into barium titanate replicas. *Journal of Materials Research*. **22,** 1121 (2007).

59. C. E. Fowler, Y. Hoog, L. Vidal and B. Lebeau: Mesopososity in diatoms via surfactant induced silica rearrangment. *Chemical Physics Letters*. **398,** 414 (2004).

60. S. Brunauer, P. H. Emmett and E. Teller: Adorption of Gases in Multimolecular Layers. *Journal of the American Ceramic Society*. **60,** 309 (1938).

61. S. H. Jhung, J.-H. Lee, J. W. Yoon, Y. K. Hwang, J.-S. Hwang, S.-E. Park and J.-S. Chang: Effects of reaction conditions in microwave synthesis of nanocrystalline barium titanate. *Materials Letters*. **58,** 3161 (2004).

62. K. Uchino, E. Sadanaga and T. Hirose: Dependence of the Crystal Structure on Particle Size in Barium Titanate. *Journal of the American Ceramic Society*. **72,** 1555 (1989).

63. B. D. Begg, E. R. Vance and J. Nowotny: Effect of Particle Size on the Room-Temperature Crystal Structure of Barium Titanate. *Journal of the American Ceramic Society*. **77,** 3186 (1996).

64. K. Kinoshita and A. Yamaji: Grain-size effects on dielectric properties in barium titanate ceramics. *Journal of Applied Physics*. **47,** 371 (1976).

65. H. Xu, L. Gao and J. Guo: Preparation and characterizations of tetragonal barium titanate powders by hydrothermal method. *Journal of the European Ceramic Society*. **22,** 1163 (2002).

66. E. P. Barrett, L. G. Joyner and P. P. Halenda: The Determination of Pore Volume and Area Distributions in Porous Substances. I. Computations from Nitrogen Isotherms. *Journal of the American Ceramic Society*. **73,** 373 (1951).

67. I. J. Clark, T. Takenuchi, N. Ohtori and D. C. Sinclair: Hydrothermal synthesis and characterisation of $BaTiO_3$ fine powders: precursors, polymorphism and properties. *Journal of materials Chemistry*. **9,** 83 (1999).

68. B. L. Newalker, S. Komarnemi and H. Katsuki: Microwave-hydrothermal synthesis and characterization of barium titanate powders. *Materials research Bulletin*. **36,** 2347 (2001).

69. E. Ciftci, M. N. Rahaman and M. Shumsky: Hydrothermal precipitation and characterization of nanocrystalline $BaTiO_3$ particles. *Journal of Materials Science*. **36,** 4875 (2001).

70. D. Hennings and S. Schreinemacher: Characterization of Hydrothermal Barium Titanate. *Journal of the European Ceramic Society*. **9,** 41 (1992).

71. R. Asiaie, W. Zhu, S. A. Akbar and P. K. Dutta: Characterization of Submicron Particles of Tetragonal $BaTiO_3$. *Chemistry of Materials*. **8,** 226 (1996).

72. H. M. O'Bryan and J. Thomson: Phase Equilibria in the TiO_2-Rich Region of the System BaO-TiO_2. *Journal of the American Ceramic Society*. **57,** 522 (1974).